

Crash Behavior of Box Columns Filled with Aluminum Honeycomb or Foam

by

Sigit P. Santosa

Ir., Bandung Institute of Technology

Submitted to the Department of Mechanical Engineering
in partial fulfillment of the requirements for the degree of

Master of Science in Mechanical Engineering

at the

MASSACHUSETTS INSTITUTE OF TECHNOLOGY

May 1997

© Massachusetts Institute of Technology 1997. All rights reserved.

Author

Department of Mechanical Engineering

May 20, 1997

Certified by

Tomasz Wierzbicki

Professor of Applied Mechanics

Thesis Supervisor

Read by

Frank A. Mc Clintock

Professor of Mechanical Engineering

Thesis Reader

Accepted by

Prof. Ain A. Sonin.

Chairman, Mechanical Engineering Graduate Committee

MASSACHUSETTS INSTITUTE
OF TECHNOLOGY

JUL 21 1997

ARCHIVES

LIBRARIES

Crash Behavior of Box Columns Filled with Aluminum Honeycomb or Foam

by

Sigit P. Santosa

Submitted to the Department of Mechanical Engineering
on May 20, 1997 , in partial fulfillment of the
requirements for the degree of
Master of Science in Mechanical Engineering

Abstract

The effect of low density filler material, such as aluminum honeycomb or foam, is studied on the axial crushing resistance of a square box column under quasi-static loading. Crushing strength of light weight filler is first studied analytically and numerically. Then, the conditions for contact between the column walls and metal filler are formulated to properly model the strengthening interaction. A simple relationship between mean crushing force and the strength of filler is developed from this study. Numerical simulation shows that, in terms of achieving the highest strength to weight ratio, filling the box column with aluminum honeycomb which has a solidity ratio greater than 1.2 % is preferable to thickening the column wall. Superior strength to weight ratio is also obtained by filling the column with aluminum foam which has solidity ratio greater than 2.3 % . These non-bonded results are improved by 40 % in the presence of adhesive.

Thesis Supervisor: Tomasz Wierzbicki
Title: Professor of Applied Mechanics

Acknowledgments

First and foremost, I would like to express my deepest gratitude to my advisor, Professor Tomasz Wierzbicki, for his invaluable guidance and assistance with this research. His dedication to further the engineering profession was inspiring. I only hope that I can live up to the high standards set by his example. I would also like to thank Prof. Frank A. Mc Clintock for his helpful discussion in finishing this thesis.

I am also grateful to Dr. Anand Tanavde from ESI Group Software Co., Detroit, for providing an assistance in running the finite element code PAM CRASHTM. Without him, I would not have found all my simulation problems. Thanks are also due to Anthony Simone of The Department of Civil Engineering MIT for his helpful information on the newly developed material aluminum foam. I'd also like to thank my colleagues in the Impact & Crashworthiness Laboratory at MIT, Jay Falls, and Chiara Bisagni, for their help, encouragement, and friendship.

This last group of people has the greatest influence on my life. My father, Soewardi, and my late mother, Sri Soeratmi, have supported me emotionally throughout my academic career. To them I own a heart felt thank you. I also owe my gratitude to my brothers Widiyatmo, Heru Prasetya, and Wiratmoko, and my sisters Titik and Endah, who were always supportive. Lastly, and in my heart the most important, I would like to thank my wife, Erna. Without her love, support, and patience, "our" master degree would not have been reality. She gave me a special gift, the precious son Arsyad Parama Santosa, during my stay at MIT. I'm looking forward to a wonderful life together.

Contents

1	Introduction	6
1.1	Research Objective	9
1.2	Scope of Present Research	9
2	Superfolding Element	11
2.1	Basic folding mechanism	11
2.2	Displacement and velocity fields	14
2.3	Principle of virtual velocity	14
2.4	Internal energy dissipation	16
2.5	Governing equation for a single superfolding element	21
3	Theoretical Prediction on the Crushing Resistance	23
3.1	Crushing strength of a square box column	23
3.2	Crushing resistance of aluminum honeycomb	25
3.3	Crushing resistance of aluminum foam	28
3.3.1	Crushing resistance of cruciform section	30

3.3.2	Strengthening effect of web and pyramidal sections	32
3.3.3	Numerical analysis of the truncated cube model	33
4	Finite Element Modeling	38
4.1	Mesh size	38
4.2	Geometric boundary conditions	40
4.3	Contact interfaces	40
4.3.1	Sliding interfaces	40
4.3.2	Tied contact	43
4.4	Time step and mass scaling	43
4.5	Velocity boundary condition	44
4.6	Material Properties	45
4.6.1	Aluminum extrusion properties	45
4.6.2	Aluminum honeycomb properties	45
4.6.3	Aluminum foam properties	47
4.6.4	Adhesive properties	48
5	Simulation Results on the Crash Behavior of Filled-Box Columns	49
5.1	Metal filler orientation	50
5.1.1	Crushing load and fold formation	51
5.1.2	Deformation pattern of filled-box column	55
5.1.3	Energy absorption characteristics	57

5.1.4	Mean crushing load	58
5.2	Effect of crushing strength of metal filler	61
5.2.1	Crushing load characteristics	62
5.2.2	Energy absorption characteristics	63
5.2.3	Mean crushing load	64
5.3	Effect of adhesive	66
5.3.1	Crash behavior characteristics	69
5.4	Specific energy absorption	70
6	Discussion and Conclusion	75
6.1	Selection of metal filler	76
6.2	Effect of adhesive	77
6.3	Future study	78

List of Figures

1.1	Mechanical response of aluminum foam (compressive)	7
2.1	Deformation pattern (a) and basic folding mechanism (b) in superfolding element	12
2.2	Global geometry of the basic folding mechanism (a) and plastic flow of a metal sheet through a toroidal surface (b)	17
3.1	Honeycomb cell structure	26
3.2	Crushing resistance of 5056 aluminum honeycomb	28
3.3	Morphology of closed-cell aluminum foam	29
3.4	Truncated cube model for foam: (i) an assembly of foam cell, (ii) and (iii) Basic folding element	30
3.5	Finite element model of foam cell: (a) Initial state, (b) partially crushed state	34
3.6	Non-dimensional crushing strength of truncated cube model	35
3.7	Crushing resistance of HYDRO foam	36
4.1	Square box column with honeycomb filler	39
4.2	Constitutive modeling of material 41	46

5.1	Crushing load characteristics for all types of filling (50 psi)	51
5.2	Unidirectional strengthening with aluminum honeycomb filling	53
5.3	2-D Lateral strengthening of box column	54
5.4	Deformation pattern of filled box column	55
5.5	Deformation pattern of foam-filled and empty box column	56
5.6	Energy absorption characteristics of filled-box column	57
5.7	Mean crushing load of filled-box column	59
5.8	Crushing load characteristics for different strength of metal filler	61
5.9	Energy absorption for different strength of metal filler	62
5.10	Mean crushing load versus crush distance for different strength of metal filler	64
5.11	Mean crushing load for different strength of metal filler	66
5.12	Symmetric (extensional) folding mode with adhesive without imperfections .	67
5.13	Asymmetric (quasi-extensional) folding mode with adhesive induced by trig- gering imperfection	67
5.14	Crushing load characteristics for filled box column with adhesive	68
5.15	Energy absorption and mean crushing load with adhesive	69
5.16	Specific energy absorption for different strengthening methods	73

Chapter 1

Introduction

In the design of metallic energy dissipating structures, the concept of a space frame composed of thin-walled prismatic columns, has been identified as a very efficient impact energy absorbing system, [1]. In this type of structure, energy absorption will normally take place by a combination of progressive folding and bending collapse of the prismatic column. For light weight designs, low density metal filler, such as aluminum honeycomb or foam, has potential for increasing energy absorption of a thin-walled prismatic column. The increase of energy will be absorbed by the large compressive deformation of the filler. A fundamental theoretical study on the crash behavior of hexagonal cell structures for honeycomb was published in [2]. Closed-form solutions for deformation, force resistance, and energy absorption of a sandwich plate with a honeycomb core were derived by Wierzbicki *et.al.*, [3].

Recent developments of cost-effective processes for the production of low density cellular materials, such as aluminum foam, have cleared the way for using it in energy absorption devices to reinforce a space frame structure, [4]. As also observed in the honeycomb structure, aluminum foam shows a typical behavior of highly porous cellular solids: an initial approximately linear elastic regime is followed by an extended plastic plateau, truncated by

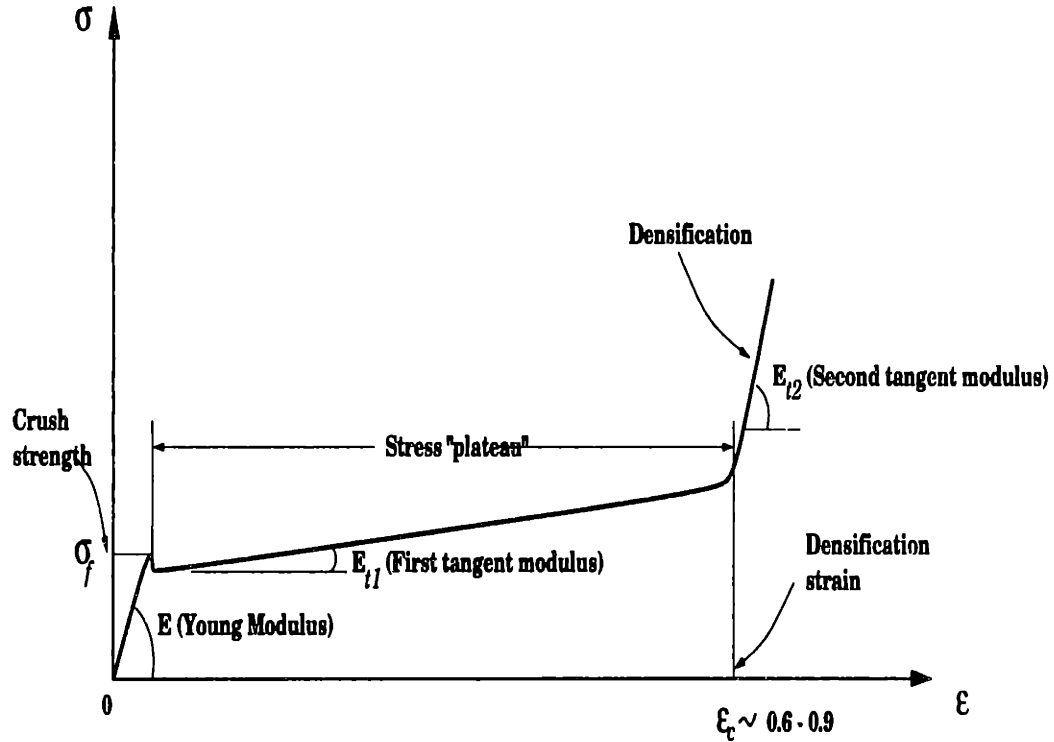


Figure 1.1: Mechanical response of aluminum foam (compressive)

a densification response at high strains during which the stress again increases steeply, as shown in Fig. 1.1. Deformation of structural foam occurs by progressive collapse of individual cells through the thickness of the body. This results in an exceptionally large compressive strain, approaching 80 %. For this reason, structural foam has potential for use in applications which require superior impact energy absorption, particularly those applications which would benefit from significant reductions in component weight. An experimental study on the crash behavior of aluminum extrusion filled with aluminum foam has recently been initiated by Hanssen and Langseth, [5], at the Norwegian Institute of Technology. Their work lays a foundation for the development of aluminum based crash absorption components.

The crash behavior of a hollow thin-walled column has been studied extensively in the literature. Of interest in these studies were the force-displacement with the mean crushing

force P_m and the energy absorption. A classical analysis of plastic folding of a thin cylindrical shell under axial crush loading goes back to the work of Alexander in 1960, [6]. A theoretical analysis of the plastic deformation of a prismatic column undergoing static compression load was developed by Wierzbicki and Abramowicz, [7]. In their method, the deformed section was analyzed by using *superfolding element* which is basically a two-degrees of freedom corner element. The experimental validation of the proposed theory was performed by Abramowicz and Jones, [8]. In their work, they also studied the dynamic crushing strength of columns. For a specific material, complete static and dynamic axial crushing tests of square thin-walled aluminum extrusion were conducted by, among others, Langseth *et.al.*, [9].

The effect of filling metal tube with low density material was first studied for polyurethane foam. It has been observed that foam-filling can be preferable to increasing the wall thickness in terms of achieving the same energy absorption. In very thin cylindrical tubes ($D/t > 500$), the foam prevented irregular overall buckling and forces the development of more symmetric stable buckling patterns, as shown by the study of Reddy and Wall, [10]. These authors found that stability of the crushing process was also improved by the presence of the filler. In their analysis, the contribution of energy absorption from the foam was considered to be independent from the deformed geometry of the tube.

An iterative method of treating progressive folding of foam-filled prismatic column was independently developed by Abramowicz and Wierzbicki, [11]. In their analysis, the coupling between the deformation of the column and the foam was considered. This approach led a shorter, more realistic folding length. Their theoretical prediction on the crash behavior of foam-filled section showed good agreement with the available experimental results.

1.1 Research Objective

The objective of this research is to predict crash behavior of thin-walled column filled with low density aluminum based material. The increase of energy absorption for different metal filler and material properties orientation is studied and compared with the conventional method of thickening the column wall. Numerical simulation then determines an efficient energy absorber from various strengthening methods. Simple analytical formulas for mean crushing load and specific energy absorption are also derived based on the analytical and numerical results.

1.2 Scope of Present Research

Crushing strength of light weight filler is studied analytically and numerically. This will include the analytical prediction on the crushing strength of aluminum honeycomb and foam. Theoretical prediction of aluminum honeycomb crushing strength has been developed in [2] and gives an excellent agreement with the experimental test results, [3], [12]. On the other hand, no theoretical prediction is available for the crushing strength of closed-cell aluminum foam. The only available theoretical analysis of foam structure is based on the cellular material developed by Gibson and Ashby [13]. However, as shown by Kunze *et.al.*, [4], and Simone and Ashby, [14], the prediction for foam structure underestimates the experimental results. This is due to the fact that the original model is based on the cubic model of cellular material and that the true cell structure is polygonal with a combination of larger and smaller cells. Therefore, this research will also develop a new crushing strength formulation for closed-cell foam structure. The theoretical analysis of metal fillers, along with the theoretical analysis of square box column, are used to predict the crash behavior of filled-box column to be compared with the numerical analysis.

In the numerical analysis of filled-box column, the non-linear finite element code PAM-CRASHTM is used. A square box column is first filled with 0.345 MPa (50 psi) aluminum honeycomb to quantify the strengthening effect in axial direction and subsequently in lateral direction of the column. The numerical analysis also simulates a “hypothetical” honeycomb which has strong mechanical properties in two orthogonal directions. This type of honeycomb is needed to determine the strengthening effect due to the lateral support on the column wall. Finally, aluminum foam filling which has approximately the same strengthening in all three orthogonal directions is studied. The effect of various strengths of metal filler and adhesive between the column wall and metal filler is also assessed in this study.

In Chapter 2, the governing energy balance equation for a superfolding element is formulated. The governing equation is then used to derive the crushing strength of a square box column and metal filler outlined in Chapter 3. In this chapter, a new theoretical analysis on the crushing strength of foam structure based on a truncated cube model is developed. Chapter 4 lays out the finite element modeling for filled box column. The numerical results are given in Chapter 5. In this chapter, simple formulas for the crushing strength and specific energy absorption of a square box column filled with honeycomb and foam structure are developed. Finally, Chapter 6 discusses the strengthening mechanism of a prismatic box column from the point of weight efficiency and outlines future research.

Chapter 2

Superfolding Element

Analytical technique to study crushing behavior of thin-walled structural elements is based on the superfolding element developed in [7] and [15]. Following the above references, this chapter will describe fundamental solution for a single superfolding element which can be applied to analyze crushing resistance of prismatic box column, honeycomb, and foam structure undergoing axial crushing load.

2.1 Basic folding mechanism

Progressive crushing of a prismatic column involves subsequent deformation of a consecutive layer. Two possible deformation patterns of a single layer are shown in Figure 2.1a. A superfolding element represents a segment of a corner line of the prismatic column as shown in corresponding mode of deformation. In this case, the deformation pattern in the single layer cell can be asymmetric or symmetric mode. The asymmetric mode can be referred as the quasi-inextensional deformation mode while the symmetric mode can be referred as the extensional deformation mode. There is also an inverted mode in which two adjacent walls

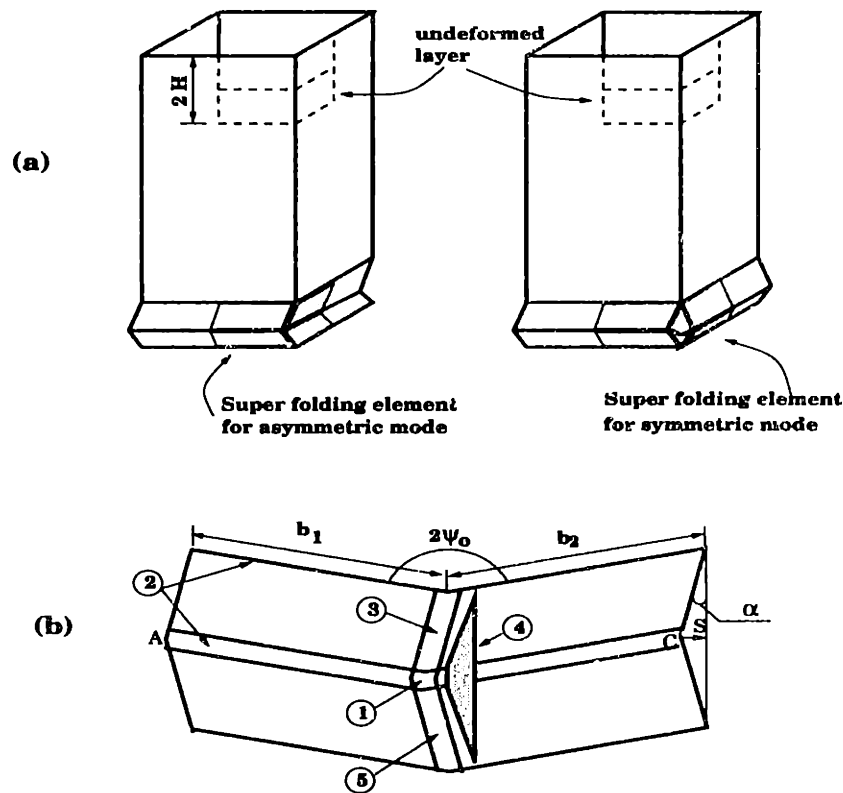


Figure 2.1: Deformation pattern (a) and basic folding mechanism (b) in superfolding element are both deforming in the inward direction.

The general deformation mode of a single superfolding element is shown schematically in Figure 2.1b. In this case, the folding mechanism in a single superfolding element is constructed from a simple folding mechanism referred to as asymmetric and symmetric deformation mode. The basic plastic folding mechanisms consists of five different deformation mechanisms, which are

1. Deformation of a floating toroidal surface
2. Bending along stationary hinge lines
3. Rolling deformations

4. Opening of a conical surface
5. Bending of deformations along inclined, stationary, hinge lines which follows locking of a traveling hinge line 3.

The asymmetric deformation mode is characterized by the absence of a conical surface (4). Consequently, the entire folding process is controlled by the propagating hinge line (3). The symmetric deformation mode, on the other hand, lacks the propagating hinge line (3). In this case, local plastic deformations are confined to the conical surface (4).

The known input parameters for the generalized folding modes are: the length of the cross-section b , ($b = b_1 + b_2$), the wall thickness t , and the angle of intersection between two side flens ψ_o . These parameters can be represented by the vector :

$$\xi = \{b, t, \psi_o\} \quad (2.1)$$

The rotation of a side face of an element from the initial upright position α is considered to be an independent variable which controls the crushing process. Parameter α is often considered as a time-like parameter. The length of the buckling wave $2H$, the small bending radius of toroidal surface r , and the switching parameter $\bar{\alpha}$ at which the conical stretching is activated are all unknown and determined as a part of the solution. These unknown parameters can be written as a vector of free parameters:

$$\chi = \{H, r, \bar{\alpha}\} \quad (2.2)$$

2.2 Displacement and velocity fields

The kinematically admissible displacement field of a single superfolding element is described by a vector

$$u = u(x, \chi, \alpha) \quad (2.3)$$

where x is the spatial position of a given particle. The velocity field :

$$\dot{u} = \dot{u}(x, \chi, \alpha)\dot{\alpha} \quad (2.4)$$

which is obtained from the displacement field by time differentiation, is piecewise continuous. Thus, the lines of the slope discontinuities, representing plastic hinge lines, are admitted.

Assuming that the column is subjected to a uniform compression between rigid plates and that only one fold is formed at a time, the shortening of superfolding element δ is related to the rotation of the side panels α by

$$\delta = 2H(1 - \cos\alpha) \quad (2.5)$$

where $2H$ is the length of the folding wave. The rate form of the above equation is

$$\dot{\delta} = 2H(\sin\alpha)\dot{\alpha}. \quad (2.6)$$

The horizontal displacement and velocity of point C are given by

$$S = H\sin\alpha \quad (2.7)$$

$$\dot{S} = V = H(\cos\alpha)\dot{\alpha} \quad (2.8)$$

2.3 Principle of virtual velocity

The equilibrium of a superfolding element is expressed via the principle of virtual velocities. For axial crushing process, which is a one-dimensional problem, the virtual velocity

principle can be written in the form :

$$P\dot{\delta} = \int_V \sigma \cdot \dot{\epsilon} dV \quad (2.9)$$

where $\dot{\delta}$ is a prescribed velocity of an axial compression process, P is the resisting axial force, while σ and $\dot{\epsilon}$ are the statically and kinematically admissible fields, respectively. The product $P\dot{\delta}$ represents the rate of work of external forces where the relative velocity of the uniformly shortened upper and lower edges of the basic folding mechanism is denoted by $\dot{\delta}$, while P is the instantaneous crushing force. This force is equilibrated by the system of internal stresses σ .

The total plastic work is proportional to the mean crushing force P_m , defined by integrating equation (2.9) with respect to the process parameter from $\alpha = 0$ to $\alpha = \alpha_f$

$$P_m \delta_{ef} = \int_0^{\alpha_f} d\alpha \int_V \sigma \dot{\epsilon} dV \quad (2.10)$$

The best set of parameter H, τ is obtained by extremizing the rate of energy dissipation with respect to the vector of free parameters :

$$\frac{\partial}{\partial \chi} \int_V \sigma \dot{\epsilon} dV = 0. \quad (2.11)$$

Integrating equation (2.11) with respect to time (or α) from $t = \alpha = 0$ to the end process $t = t_f, \alpha = \alpha_f$ and changing the order of integration, it gives

$$\frac{\partial}{\partial \chi} \int_0^{\alpha_f} d\alpha \int_V \sigma \dot{\epsilon} dV = 0. \quad (2.12)$$

Using equation (2.10), the condition in equation (2.12) is equivalent to the extremization of the mean crushing force :

$$\frac{\partial}{\partial \chi} P_m(\chi, \alpha_f) = 0 \quad (2.13)$$

2.4 Internal energy dissipation

The rate of internal energy dissipation in a deformed superfolding element results from the continuous and discontinuous velocity fields is

$$\dot{E}_{int} = \int_S (M_{\alpha\beta} \dot{\kappa}_{\alpha\beta} + N_{\alpha\beta} \dot{\epsilon}_{\alpha\beta}) dS + \sum_{i=1}^n \int_{L_i} M_o^i [\dot{\theta}_i] dl^i, \quad (2.14)$$

where S denotes the current shell mid surface, n is the total number of plastic hinge lines, L_i is the length of the i_{th} hinge, and $[\dot{\theta}_i]$ denotes a jump of the rate of rotation across the moving hinge line. The components of the rate of rotation and the rate of extension tensors are denoted as $\dot{\kappa}_{\alpha\beta}$ and $\dot{\epsilon}_{\alpha\beta}$, respectively. The corresponding conjugate generalized stresses are the bending moments $M_{\alpha\beta}$ and the membrane forces $N_{\alpha\beta}$. The total internal plastic dissipation is obtained by integrating equation (2.14) in the interval $0 \leq \alpha \leq \alpha_f$. Since the total dissipation is obtained as a result of two different folding modes acting in series, the expression for the rate of energy splits into two parts :

$$E_{int} = \int_0^{\bar{\alpha}} \dot{E}_{int}^{(1)} d\alpha + \int_{\bar{\alpha}}^{\alpha_f} \dot{E}_{int}^{(2)} d\alpha \quad (2.15)$$

where $\bar{\alpha}$ denotes a configuration at which the extensional mode of deformation takes over the quasi-inextensional mode.

During the first phase of the deformation $0 \leq \alpha \leq \bar{\alpha}$, the crushing process is controlled by a quasi-inextensional folding mode and the corresponding dissipation is due to plastic flow over the toroidal surface and the bending along stationary and traveling hinge lines.

Consider first the plastic flow over toroidal surface in Figure 2.2. The integrand in the first integral of equations (2.14) has, in general, six components. In view of the rotational symmetry and the assumed radial plastic flow, all non-diagonal components of the strain rate tensor ($\dot{\kappa}_{\theta\Phi}, \dot{\epsilon}_{\theta\Phi}$) vanish. The stretching rate $\dot{\lambda}_{\theta\theta}$ in the meridional direction is assumed

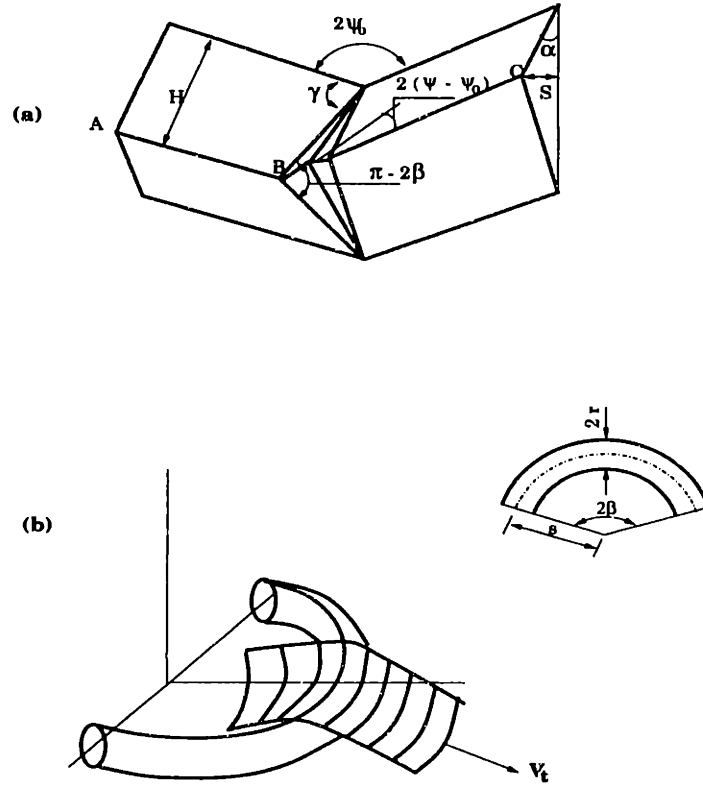


Figure 2.2: Global geometry of the basic folding mechanism (a) and plastic flow of a metal sheet through a toroidal surface (b)

to be zero. The rate of curvature $\dot{\kappa}_{\theta\theta}$ equals to zero under the assumption of central velocity field, [7], with the tangential velocity V_t . The remaining components of the stretching and curvature tensors are :

$$\dot{\lambda}_{\Phi\Phi} = -\frac{\dot{\omega}rs\sin\theta}{x}, \quad (2.16)$$

$$\dot{\kappa}_{\Phi\Phi} = -\frac{\dot{\omega}ss\sin\theta}{x^2} \quad (2.17)$$

where r and s denote, respectively, smaller and larger radius of the toroidal surface, and x is a current position of the point with θ coordinate with respect to the axis of symmetry. The tangential velocity is related to the horizontal velocity V in equation (2.8) by

$$V_t = \dot{\omega}r = \frac{V}{tg\psi_0} \quad (2.18)$$

In the case of rotationally symmetric shells with only two non-vanishing components of the generalized strain rate tensor, the yield condition has the form

$$\left| \frac{M_{\Phi\Phi}}{M_o} \right| + \left(\frac{N_{\Phi\Phi}}{N_o} \right)^2 = 1 \quad (2.19)$$

where $M_o = \frac{1}{4}\sigma_o t^2$, and $N_o = \sigma_o t$. Here the material is assumed as rigid-perfectly plastic, isotropic and independent of time with a suitably adjusted flow stress σ_o to account for work-hardening properties of material.

The surface element in (2.14) is expressed as

$$dS = x \, d\Phi \, r \, d\theta \quad (2.20)$$

and the limits of integration are

$$\frac{\pi}{2} - \psi \leq \theta \leq \frac{\pi}{2} + \psi \quad (2.21)$$

$$-\beta < \Phi < \beta \quad (2.22)$$

where 2β is a central angle of toroidal section, and the angle ψ is linearly increasing with Φ from ψ_o to $\frac{\pi}{2}$ according to

$$\psi = \psi_o + \frac{\pi - 2\psi_o}{\pi} \Phi \quad (2.23)$$

It follows from the flow rule, [7], that if the ratio of the larger and smaller radius of toroidal section greater than 2, i.e. $\frac{s}{r} \geq 2$, the stress profile is confined to the point $N_{\Phi\Phi} = N_o$, $M_{\Phi\Phi} = 0$, The first integral in (2.14) is then reduced to

$$\dot{E}_1 = \int_{-\beta}^{\beta} r \left\{ \int_{\frac{\pi}{2}-\psi}^{\frac{\pi}{2}+\psi} \left[N_o \frac{\dot{\omega} r \sin\theta}{x} \right] x d\theta \right\} d\Phi \quad (2.24)$$

The first integration gives

$$\dot{E}_1 = \int_{-\beta}^{\beta} 2\dot{\omega} r^2 N_o \sin\psi \, d\Phi \quad (2.25)$$

With the help of (2.8) and (2.18), the above integration can be performed to obtain :

$$\dot{E}_1 = \frac{4N_o r H \pi}{(\pi - 2\psi_o) \operatorname{tg} \psi_o} \cos \alpha \left\{ \sin \psi_o \sin \left(\frac{\pi - 2\psi_o}{\pi} \right) \beta + \cos \psi_o \left[1 - \cos \left(\frac{\pi - 2\psi_o}{\pi} \right) \right] \beta \right\} \dot{\alpha} \quad (2.26)$$

Integrating over the whole deformation process, the work done on a complete folding of the element through the angle $\bar{\alpha}$ is

$$E_1 = 4HrN_o I_1(\psi_o) = 16M_o H \frac{r}{t} I_1(\psi_o) \quad (2.27)$$

where I_1 is defined by

$$I_1(\psi_o) = \frac{\pi}{(\pi - 2\psi_o) \operatorname{tg} \psi_o} \int_0^{\bar{\alpha}} \cos \alpha \left\{ \sin \psi_o \sin \left(\frac{\pi - 2\psi_o}{\pi} \right) \beta + \cos \psi_o \left[1 - \cos \left(\frac{\pi - 2\psi_o}{\pi} \right) \right] \beta \right\} d\alpha \quad (2.28)$$

The two angles γ and β are related to ψ_o and α through

$$\operatorname{tg} \gamma = \frac{\operatorname{tg} \psi_o}{\sin \alpha}, \quad \operatorname{tg} \beta = \frac{\operatorname{tg} \gamma}{\sin \psi_o} \quad (2.29)$$

Since, according to (2.29), the angle β is a function of α , the integration in (2.28) is a known function of the angle ψ_o .

The rate of energy dissipated on the horizontal hinge lines \dot{E}_2 equals to the limit bending moment per unit length M_o times the rate of rotation α times the length of the hinge b ,

$$\dot{E}_2 = 2M_o b \dot{\alpha}. \quad (2.30)$$

The total energy dissipation, obtained by integrating the above equation in the limit of $(0, \bar{\alpha})$ is

$$E_2 = 2M_o b \bar{\alpha}. \quad (2.31)$$

The rate of energy due to the inclined traveling hinge lines is equal to the fully plastic bending moment times the rate of rotation $\dot{\omega}$ times the variable length of the hinge line

$l = \frac{2H}{\sin\gamma}$. This gives

$$\dot{E}_3 = 4M_o \frac{H^2}{r} \operatorname{ctg}\psi_o \cos\alpha \sqrt{(tg^2\psi_o + \sin^2\alpha)} \dot{\alpha}. \quad (2.32)$$

The total energy dissipation is then

$$E_3 = 4M_o \frac{H^2}{r} I_3(\psi_o) \quad \text{where} \quad (2.33)$$

$$I_3(\psi_o) = \operatorname{ctg}\psi_o \int_0^{\bar{\alpha}} \cos\alpha \sqrt{tg^2\psi_o + \sin^2\alpha} d\alpha \quad (2.34)$$

In the second phase of crushing process $\bar{\alpha} \leq \alpha \leq \alpha_f$, the crushing process is controlled by extensional folding mode. In this stage, the conical surface is formed. It is assumed that material within the conical zone undergoes stretching in the direction of θ and is in-extensible in the second principal direction. The rate of energy dissipated in the conical zone is defined by

$$\dot{E}_4 = \int_S N_o \dot{\lambda}_{\theta\theta} dS \quad (2.35)$$

where S is a current area of the growing cone which uniquely depends on α . The total energy dissipation is

$$E_4 = 4M_o \frac{H^2}{t} I_4(\psi_o) \quad \text{where} \quad (2.36)$$

$$I_4 = \int_{\bar{\alpha}}^{\alpha_f} \frac{\sin\bar{\alpha} \operatorname{tg}\psi_o \sin 2\alpha}{2(\sin^2\bar{\alpha} + tg^2\psi_o \sin^2\alpha)} + (\psi - \psi_o) \cos\alpha d\alpha \quad (2.37)$$

The rate of energy dissipation on the horizontal hinge line is the same as in the phase I. The total energy is

$$E_5 = 2M_o b(\alpha_f - \bar{\alpha}) \quad (2.38)$$

During the second phase of deformation, the inclined hinge line is fixed in a material coordinate system and has constant length. The corresponding contribution to the rate of

energy dissipation comes from bending in the stationary hinge line which is

$$\dot{E}_6 = 2M_o H \operatorname{ctg}\psi_o \frac{\sin\bar{\alpha}(\sin^2\bar{\alpha} + tg^2\psi_o)}{\sin^2\bar{\alpha} + tg\psi_o \sin^2\alpha} \dot{\alpha} \quad (2.39)$$

The total energy is obtained by integrating the above equation in the limits $(\bar{\alpha}, \alpha_f)$,

$$E_6 = M_o H I_6(\psi_o) \quad (2.40)$$

where

$$I_6 = 2 \operatorname{ctg}\psi_o \int_{\bar{\alpha}}^{\alpha_f} \frac{\sin\bar{\alpha}(\sin^2\bar{\alpha} + tg^2\psi_o)}{\sin^2\bar{\alpha} + tg\psi_o \sin^2\alpha} d\alpha \quad (2.41)$$

For each given value of the angle ψ_o , the definite integrals I_1 through I_6 can be evaluated numerically if the magnitude of switching point $\alpha = \bar{\alpha}$ is known. In the case of crushing process involving only one deformation mode, the definite integrals can be evaluated in a closed form.

2.5 Governing equation for a single superfolding element

The energy balance in equation (2.10) can be obtained by summing up all the contributions of plastic mechanism of E_1 through E_6 . Each contributing term has a different functional dependence on unknown parameters r and H , so that the governing equation (2.10) can finally be written in the form :

$$\frac{P_m}{M_o} = \left\{ A_1 \frac{r}{t} + (A_2 + A_5) \frac{b}{H} + A_3 \frac{H}{r} + A_4 \frac{H}{t} + A_6 \right\} \frac{2H}{\delta_{ef}} \quad (2.42)$$

where the coefficients A_i depend on $\bar{\alpha}$ and ψ_o . A_2 and A_4 can be calculated as a closed-form functions of geometrical parameters, while A_1 and A_3 are functions of elliptic integrals and must be calculated numerically.

The effective crushing distance δ_{ef} can be calculated from the terminal shape of completely squeezed corner elements by assuming that the actual pattern of deformed corner line is composed of alternating circular arcs. It can be shown through simple calculations performed for a right angle element that $\delta_{ef}/2H = 0.73$, [16].

The mean crushing load P_m is thus a function of two unknown parameters H and r , which are determined from condition (2.13) as :

$$\frac{\partial P_m}{\partial H} = 0; \quad \frac{\partial P_m}{\partial r} = 0. \quad (2.43)$$

The crushing response of a single layer of folds is calculated by summing up fractional contribution of all corner elements in a given layer. The application of superfolding element to calculate the crushing strength of prismatic columns will be assessed further in the next chapter.

Chapter 3

Theoretical Prediction on the Crushing Resistance

This chapter will present theoretical prediction for the crushing resistance of prismatic column and metal filler. The theoretical analysis is based on the governing equation of superfolding element described in the previous chapter. The derivation of crushing resistance for a square box column and honeycomb structure are based on [7] and [2], respectively. On the other hand, theoretical prediction for crushing resistance of closed-cell foam structure is newly developed as a part of contribution of this research. The crushing resistance for each type of structure will be taken as a basis for any further theoretical development.

3.1 Crushing strength of a square box column

Consider a square box column with the cross section of $b \times b$ and the thickness of t . It is assumed that the box column undergoes a pure quasi-inextensional mode. In this case, the constants A_1 , A_2 , A_3 in equation (2.42) can be calculated by setting $\bar{\alpha} = \alpha_f = \pi/2$, and

$\psi_o = \pi/4$. Using these values, the coefficients A_1 through A_3 equal to $A_1 = 4.44$, $A_2 = \pi$, and $A_3 = 2.30$. The energy balance equation in (2.42) can then be rewritten in the form :

$$\frac{P_m}{M_o} = \left\{ A_1 \frac{r}{t} + A_2 \frac{b}{H} + A_3 \frac{H}{r} \right\} \frac{2H}{\delta_{ef}} \quad (3.1)$$

Note that coefficients A_4 and A_6 in equation (2.42) are vanishing because the lower and upper limits of integration in integral I_4 and I_6 are the same.

Solution to equation (3.1) can be obtained by applying the minimum condition, equation (2.43). Hence, physically meaningful values of r and H are obtained by minimizing P_m with respect to these parameters

$$\frac{\partial P_m}{\partial r} = \frac{\partial P_m}{\partial H} = 0 \quad (3.2)$$

This leads to two simultaneous algebraic equations for r and H . The solution of this system is

$$\frac{P_m}{M_o} = 3(A_1 A_2 A_3)^{1/3} \left(\frac{b}{t} \right)^{1/3} \frac{2H}{\delta_{ef}}. \quad (3.3)$$

Since a section of square box column is composed of four basic folding elements, all energies calculated in equation (3.1) should be multiplied by four. Consequently, solution in equation (3.3) should be multiplied by four for a square box column. Using the value of effective crushing distance $\delta_{ef} = 0.73(2H)$ (see Chapter 2), the crushing strength of a square box column is then

$$\frac{P_m}{M_o} = 52.22 \left(\frac{b}{t} \right)^{1/3} \quad (3.4)$$

For rigid perfectly plastic material with constant flow stress σ_o , in which the plastic bending moment is $M_o = \sigma_o t^2/4$, the crushing resistance of a square box column can be written as

$$P_m = 13.05 \sigma_o t^{5/3} b^{1/3} \quad (3.5)$$

To take strain hardening effects into account, the energy equivalent flow stress can be calculated by using, [17] :

$$\sigma_o = (\sigma_o^1 \sigma_o^2 \sigma_o^3)^{1/3} \quad \text{where} \quad (3.6)$$

$$\sigma_o^i = \frac{2}{(\varepsilon_o^i)^2} \int_0^{\varepsilon_o^i} \sigma(\varepsilon) \varepsilon d\varepsilon \quad i = 1, 2, 3 \quad \text{and} \quad (3.7)$$

$$\varepsilon_o^1 = 0.93(t/b)^{2/3}, \quad \varepsilon_o^2 = 0.69(t/b)^{1/3}, \quad \varepsilon_o^3 = 1.3(t/b)^{1/3}. \quad (3.8)$$

The equivalent flow stress calculation described above is based on the values of maximum plastic strain for the different regions of plastic deformation.

The mean crushing force for square box column filled with metal filler can be calculated approximately by adding the resistance of empty box, equation (3.5), to a linear term representing metal filler strengthening of the form, [18] :

$$P_{m,f} = 13.05 \sigma_o t^{5/3} b^{1/3} + b^2 \sigma_f, \quad (3.9)$$

where σ_f is the compressive resistance of metal filler. This simple approximate expression is taken only by considering axial strengthening of the filler. The lateral strengthening contribution will be developed later in this study.

3.2 Crushing resistance of aluminum honeycomb

The structure of the honeycomb is regular and symmetric and thus it can be assembled from one typical folding element consisting of two angle elements joined together forming an angle of 120° ($\psi_o = \pi/3$) (Figure 3.1). In view of the periodicity of the folding mechanism, the height of a representative folding element should be equal to the length of the local buckling wave $2H$. The effective crushing distance δ_{ef} is taken to be $2H$. This is due to the fact that the honeycomb cell is so thin that upon collapse, the fold formation on the cell is almost flat.

It is assumed that the basic folding element of honeycomb structure undergoes quasi-inextensional deformation mode. In this case the constants A_i in equation (2.42) can be

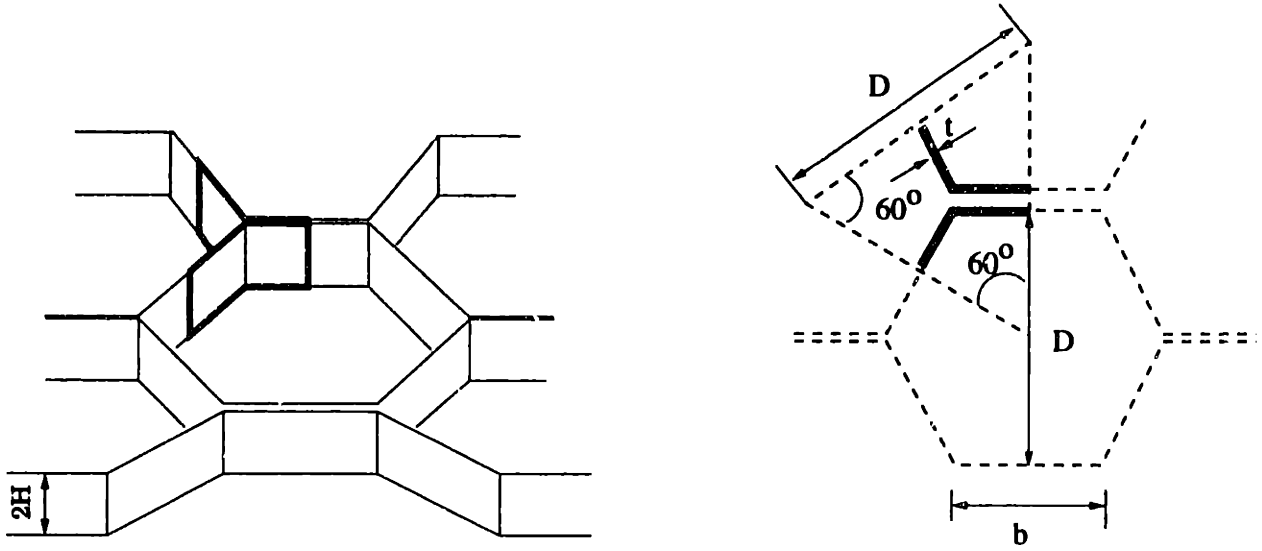


Figure 3.1: Honeycomb cell structure

calculated by using $\bar{\alpha} = \alpha_f = \pi/2$, and $\psi_o = \pi/3$.

The representative folding element has two corner so that the energy dissipated by extensional deformations in the section of a toroidal shell should be doubled which lead to the value of $A_1 = 16.8$. The energy dissipated by horizontal hinge lines should be carefully determined since a part of a typical folding element has a double thickness. The additional energy dissipated at clamped horizontal edges of the element should also be taken into account. Considering all these contributions, the horizontal hinge lines consist of : eight lines of the length $b/2$ each with $M_o = 1/4\sigma_o t^2$; four lines of the length $b/2$ each with $M_o = 1/4\sigma_o (2t)^2$. Adding all the contributing horizontal hinge lines, it gives $A_2 = 3\pi$. Finally, the energy dissipated by the inclined hinge lines should also be doubled due to the presence of two corner elements. This results in $A_3 = 9.56$

The governing energy balance equation of (2.42) for basic folding element of honeycomb structure can then be written as

$$\frac{P_m}{M_o} = \left\{ 16.8 \frac{r}{t} + 3\pi \frac{b}{H} + 9.56 \frac{H}{r} \right\} \frac{2H}{\delta_{ef}} \quad (3.10)$$

Minimizing the above governing equation with respect to the r and H , the crushing resistance of basic folding element of honeycomb structure is obtained

$$\frac{P_m}{M_o} = 34.4 \left(\frac{b}{t} \right)^{1/3} \quad (3.11)$$

Introducing the plastic bending moment and plastic flow stress of material $M_o = \sigma_o t^2/4$, the crushing resistance of basic folding element of honeycomb structure can be written as

$$P_m = 8.61 \sigma_o t^{5/3} b^{1/3} = 7.17 \sigma_o t^{5/3} D^{1/3} \quad (3.12)$$

where b and t are respectively width and thickness of the cell wall, D is the minor diameter of the cell as shown in Figure 3.1. From Figure 3.1, the “tributary” area A_s of one basic folding element is $A_s = \frac{\sqrt{3}}{4} D^2$. The crushing resistance of honeycomb structure σ_h is defined as a ratio of the mean crushing force to the tributary area, which is

$$\sigma_h = 16.55 \sigma_o \left(\frac{t}{D} \right)^{5/3} \quad (3.13)$$

It can be shown from the geometry given in Figure 3.1 that the ratio of the cross sectional area of the basic “Y” element A_h with the tributary area of one basic folding element A_s is $\frac{A_h}{A_s} = \frac{\rho_h}{\rho_s} = \frac{8}{3} \frac{t}{D}$. Hence, in terms of relative density, the crushing resistance of honeycomb can be written in the form:

$$\sigma_h = 3.22 \sigma_o \left(\frac{\rho_h}{\rho_s} \right)^{5/3} \quad (3.14)$$

Theoretical prediction for the crushing resistance is compared with recent experimental data on 5056 aluminum honeycomb reported by Hexcel Corporation, [19]. As shown in

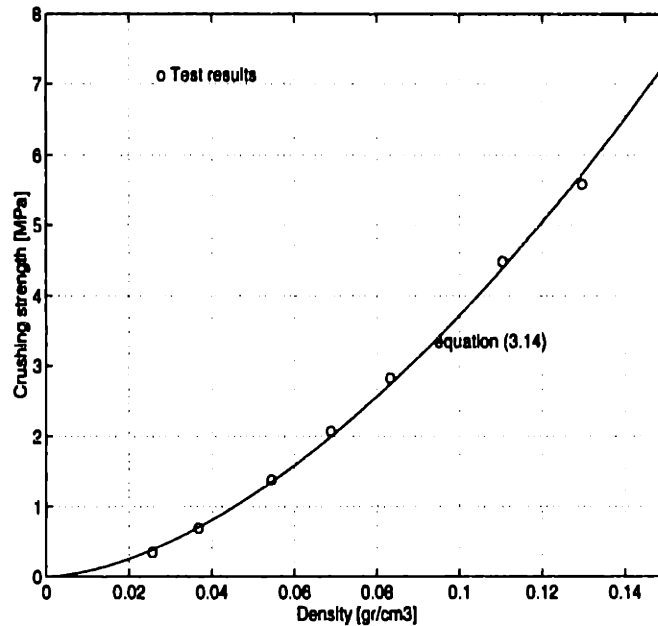


Figure 3.2: Crushing resistance of 5056 aluminum honeycomb

Figure 3.2, the correlation between the theoretical prediction and the experimental data is excellent if the flow stress is assumed to be $\sigma_o = 285$ MPa.

3.3 Crushing resistance of aluminum foam

Highly porous materials with a cellular structure such as closed-cell aluminum foam are known to have a high stiffness combined with a very low specific weight. The closed-cell aluminum foam morphology, Figure 3.3, shows that the foam has imperfections such as non-uniform cell size (multi-dispersity). The ratio between volumes of the larger and smaller cells is approximately 2 ÷ 3 order of magnitude, [20].

The structure of closed-cell foam can be approximated as a regular and symmetric unit cells assembled from a truncated cube section as shown in Figure 3.4. An assembly of

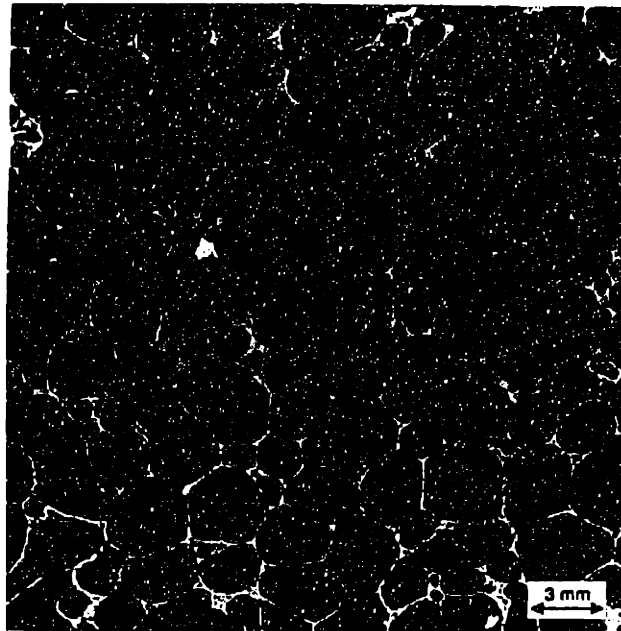


Figure 3.3: Morphology of closed-cell aluminum foam

truncated cube cells produces a realistic variation of larger and smaller foam cell structure. The basic folding element for foam structure can be taken from the symmetric part of the cell which can repeat itself to form a truncated cube model. From Figure 3.4, one typical folding element of foam structure consists of two right angle elements forming a cruciform section, pyramidal section produced by truncated cube, and web section to form a closed-cell structure.

The crushing resistance of a typical folding element for closed-cell foam structure can be obtained by first calculating the crushing resistance of cruciform section. Then, the foam strength is calculated by adding the stiffening effect produced by the web and pyramidal section .

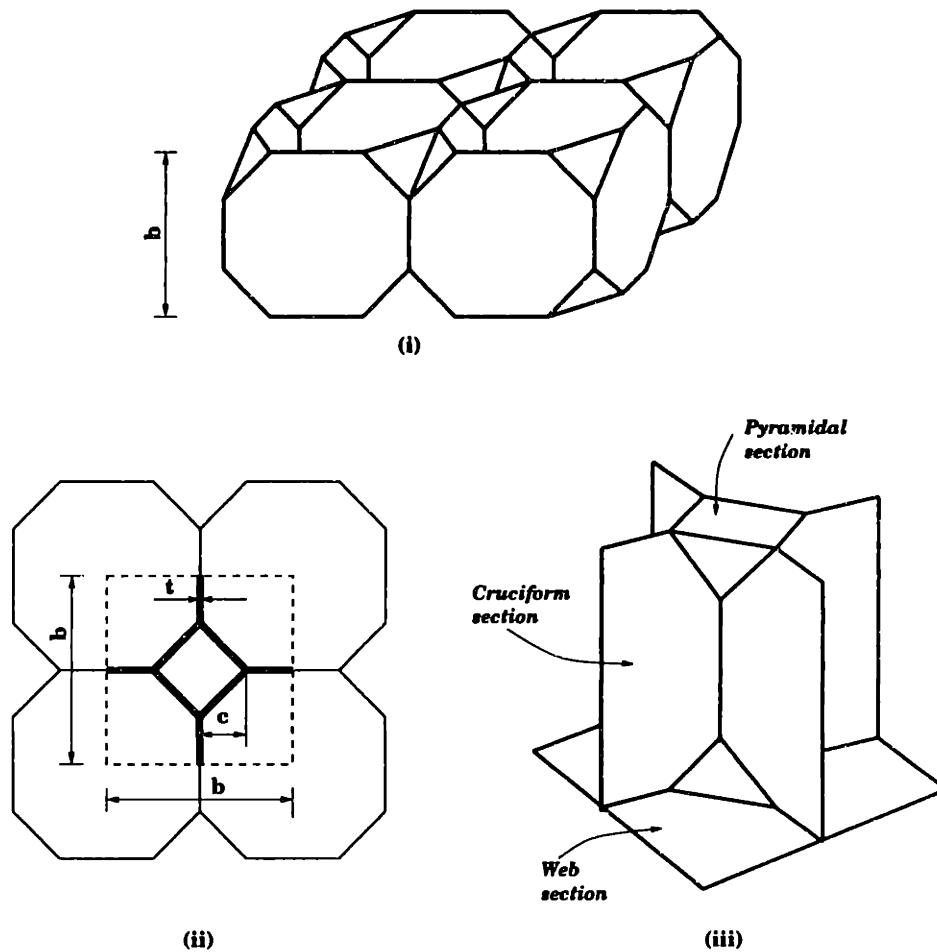


Figure 3.4: Truncated cube model for foam: (i) an assembly of foam cell, (ii) and (iii) Basic folding element

3.3.1 Crushing resistance of cruciform section

The cruciform section provides the main structure to resist the crushing load in the basic folding element of the foam structure. During the crushing process, the cruciform section collapses before the progressive folding reaches the pyramidal and web sections. A cruciform section is assembled of two right angle elements connected along a common corner line. This

connection imposes stringent constraints onto possible deformation modes of the element. In a perfect element, localized plastic deformation follows the pattern induced by the lowest elastic-plastic buckling mode. In such case, all four arms of the element buckle in the same direction and enforce development of symmetric folding pattern. This type of deformation mode is observed from the experiment, [21].

Here, the analysis follows the derivation presented in [21]. The symmetric folding mode forces the cruciform to have a pure extensional deformation pattern. Thus the constants A_i in the governing energy balance in equation (2.42) can be calculated by setting the parameter $\bar{\alpha} = 0$, $\alpha_f = \pi/2$, and the angle of intersection $\psi_o = \pi/4$. Since the cruciform consists of two right angle, the energy dissipated by horizontal hinge lines should be doubled to obtain:

$$E_5 = 2\pi M_o \sum_{i=1}^4 a_i = 2\pi M_o L \quad (3.15)$$

where $L = \sum_{i=1}^4 a_i$ is the total length of the arms of the element. The membrane energy dissipated by conical zone can be calculated as :

$$E_4 = 4\pi M_o \frac{H^2}{t} \quad (3.16)$$

Accordingly, the coefficients A_5 and A_4 in equation (2.42) which govern the extensional fold deformation are $A_5 = \pi$, $A_4 = 2\pi$. The governing energy balance equation (2.42) is then

$$\frac{P_m}{M_o} = \left\{ \pi \frac{b}{H} + 2\pi \frac{H}{t} \right\} \frac{2H}{\delta_{ef}} \quad (3.17)$$

The effective crushing distance δ_{ef} is taken to be $2H$. This is due to the fact that the foam cell is so thin that upon collapse the fold formation on the cell is almost flat. Applying the minimum condition of equation (2.43), equation (3.17) gives

$$\frac{P_m}{M_o} = 8.89 \left(\frac{L}{t} \right)^{1/2} \quad (3.18)$$

For a symmetric cruciform section, as shown in Figure 3.4, with the representative length $a_i = b/2$, the total length of the arms is $L = 2b$. Therefore, the mean crushing force of a symmetric cruciform section is

$$\frac{P_m}{M_o} = 12.57 \left(\frac{b}{t} \right)^{1/2} \quad (3.19)$$

Introducing the plastic bending moment and plastic flow stress of material $M_o = \sigma_o t^2/4$, the mean crushing force of basic folding element of cruciform section is in the form

$$P_m = 3.15 \sigma_o b^{1/2} t^{3/2} \quad (3.20)$$

From Figure 3.4, the “tributary” area of one basic folding element is $A_s = b^2$. The crushing resistance of cruciform section σ_{cf} is defined as a ratio of the mean crushing force to the tributary area, which is

$$\sigma_{cf} = \frac{P_m}{A_s} = 3.15 \sigma_o \left(\frac{t}{b} \right)^{3/2} \quad (3.21)$$

3.3.2 Strengthening effect of web and pyramidal sections

The pyramidal and web sections provide a further strengthening mechanism for the cruciform structure. The initial crushing load response on the truncated cube model is going to be same as that of the cruciform section alone. After the progressive fold reaches the pyramidal section, the crushing load increases. Finally, the web will provide stiffening mechanism to retard the successive fold formation in the adjacent cruciform structure. The crushing resistance of a closed-cell foam can be developed by understanding this crushing mechanism.

From the crushing mechanism outlined above, it is assumed that the cruciform section controls the crushing mechanism of the truncated cube model. The pyramidal and web sections only provide stiffening effect during the crushing process. Therefore, the crushing

resistance of foam structure can be expected to have similar power constant on the t/b with the cruciform section. The web and pyramidal strengthening effect is assumed to affect the proportionality constant between the crushing strength and the thickness to the cell size ratio. Hence, from equation (3.21), the crushing resistance of foam cell consists of cruciform, pyramidal, and web section can be predicted as

$$\frac{\sigma_f}{\sigma_o} = C \left(\frac{t}{b} \right)^{3/2} \quad (3.22)$$

Note that due to the strengthening effect obtained from web and pyramidal structure, the proportionality constant C is expected to be greater than 3.15.

3.3.3 Numerical analysis of the truncated cube model

Numerical analysis is conducted to obtain the proportionality constant C between the crushing resistance and the thickness to cell size ratio of truncated cube model for foam structure from equation (3.22). Since the deformation of cruciform section dominates the crushing process, the ratio of $\frac{t}{b}$ for foam cell is assumed to have the same fractional power with cruciform section ($\frac{3}{2}$). This assumption is found to be adequate as shown from the numerical result described below.

The geometrical model for foam structure is based on the basic folding element for truncated cube model shown in Figure 3.4. The cube is truncated at $c = b/4$. The column was modeled with 4-node shell element, while the connecting section with pyramidal structure is modeled with 3-node triangular element. A complete finite element model for the basic folding element of truncated cube model is given in Figure 3.5. In this analysis, three cells of truncated cube stacked vertically are considered to capture the strengthening effect of web and pyramidal structure. Clamped boundary conditions were applied at the bottom of the column. Symmetry conditions were applied on all free vertical and horizontal edges.

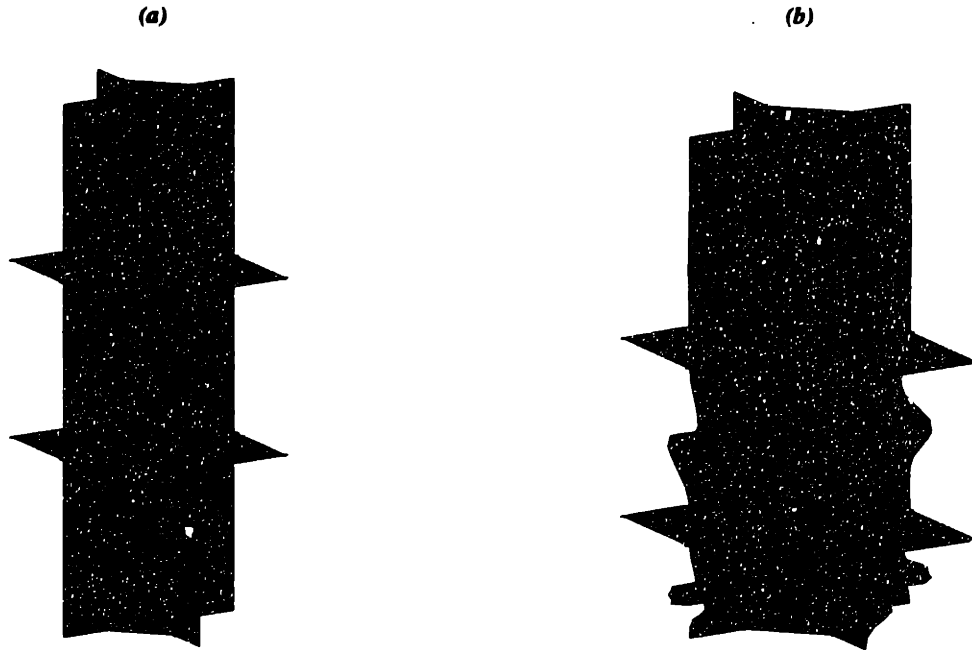


Figure 3.5: Finite element model of foam cell: (a) Initial state, (b) partially crushed state

Velocity boundary condition was applied on the top portion of the column. Velocity was ramped during the first 50 microseconds to reach constant velocity of 2 m/s . Material used in this simulation has plastic flow stress $\sigma_o = 139.2 \text{ MPa}$.

Mean crushing load from the numerical analysis is defined by :

$$P_m = \frac{1}{\delta} \int_0^\delta P(\delta) d\delta \quad (3.23)$$

where $P(\delta)$ is the instantaneous crushing load corresponding to the instantaneous shortening δ . The results of the numerical analysis for truncated cube model for different thickness to cell size ratio is given in Table 3.1. From this table, the value of the proportionality constant can be obtained as $C = 5.87$. Thus, the crushing resistance of foam structure based on the truncated cube model is

$$\frac{\sigma_f}{\sigma_o} = 5.87 \left(\frac{t}{b} \right)^{3/2} \quad (3.24)$$

Table 3.1: Crushing resistance of truncated cube model

$\frac{t}{b}$	8.75E-3	1.70E-2	2.35E-2	2.86E-2
$\frac{P_m}{\sigma_o}$	25.86	78.30	125.7	168.8
$\frac{\sigma_f}{\sigma_o}$	4.04E-03	1.22E-2	1.96E-2	2.64E-2

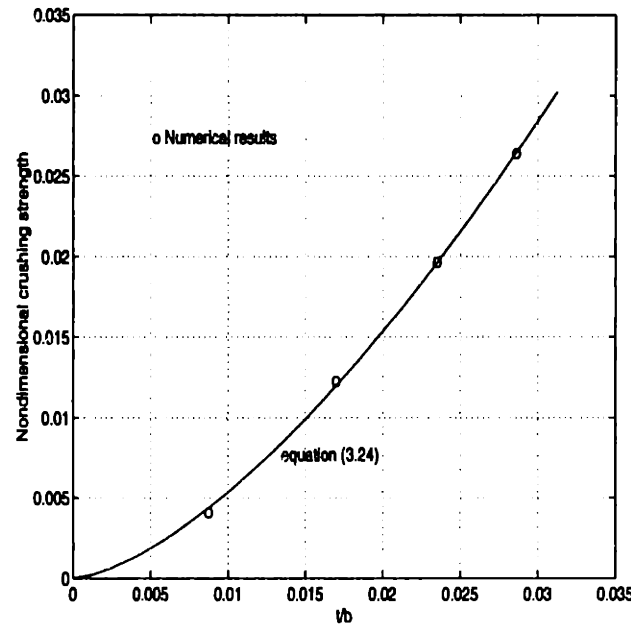


Figure 3.6: Non-dimensional crushing strength of truncated cube model

The crushing resistance of truncated cube model obtained from numerical results and equation (3.24) are plotted in Figure 3.6. Notice that the numerical results have an excellent agreement with equation (3.24). It is interesting to note that the fractional power to which the ratio of thickness to cell size for both numerical and analytical result is $\frac{3}{2}$. Therefore, the previous assumption that the cruciform section dominates the crushing process of foam cell is proven from this finding.

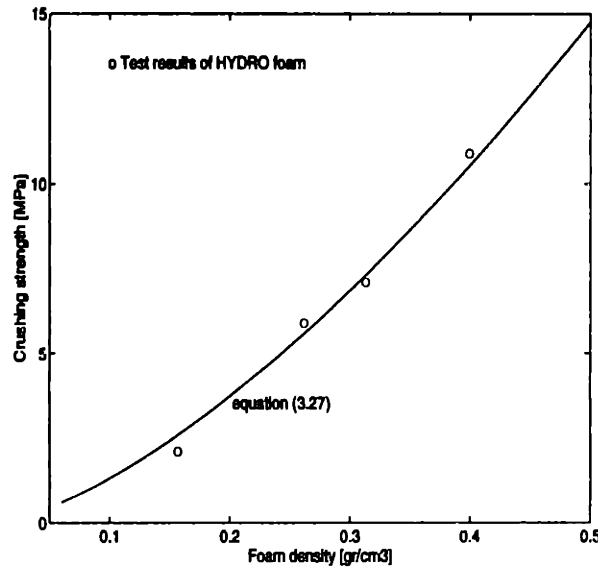


Figure 3.7: Crushing resistance of HYDRO foam

From Figure 3.4, the relative density or *solidity ratio* between the closed-cell foam and solid material for truncated cube model can be shown as

$$\frac{\rho_f}{\rho_s} = 3.5 \frac{t}{b} + (4\sqrt{3} - 7) \frac{c^2 t}{b^3} \quad (3.25)$$

For a special case with the truncated length of $c = \frac{b}{4}$, the relative density in equation (3.25) reduces to

$$\frac{\rho_f}{\rho_s} = 3.496 \frac{t}{b} \quad (3.26)$$

In terms of solidity ratio, the crushing resistance of closed-cell foam structure can then be written as :

$$\sigma_f = 0.9\sigma_o \left(\frac{\rho_f}{\rho_s} \right)^{3/2} \quad (3.27)$$

A higher crushing resistance of honeycomb over foam can be seen by comparing equations (3.14) and (3.27). The fractional power to which the relative density is raised is in both

cases almost the same (1.5 versus 1.66). However, the numerical coefficient in the solution for the honeycomb material is an order of magnitude larger than that describing the foam material. A much higher crushing resistance of honeycomb as compared to foam for the same relative density is explained by, among others, a greater degree of symmetry of the hexagonal cell structure.

Theoretical prediction for aluminum foam crushing resistance is compared with recent experimental data on HYDRO foam reported by HYDRO ALUMINIUM Co. given in Table 4.3. As shown in Figure 3.7, the correlation between the theoretical prediction and the experimental data is good if the flow stress is assumed to be $\sigma_o = 205$ MPa.

Chapter 4

Finite Element Modeling

The geometrical model was established using mesh generator program *HYPERMESH*. Finite element model was then completed with the pre-processor *PAM-GENERISTM*. Actual calculations were performed on *SGI O2* workstation with R-10000 processor using non-linear finite element code *PAM-CRASHTM*. The post-processor *PAM-VIEWTM* was used for visualization.

4.1 Mesh size

A square box column with the dimension of 80 x 80 *mm* cross section, 1.88 *mm* thickness, and 245 *mm* length was considered in this analysis. The column wall was modeled with 4-node shell element using material type 103, while the filler was modeled with 8-node solid element using material type 41.

In axial loading condition, square box column has two symmetry planes in its cross section, i.e. with respect to XoY and YoZ planes (see Figure 4.1). As a result, structural

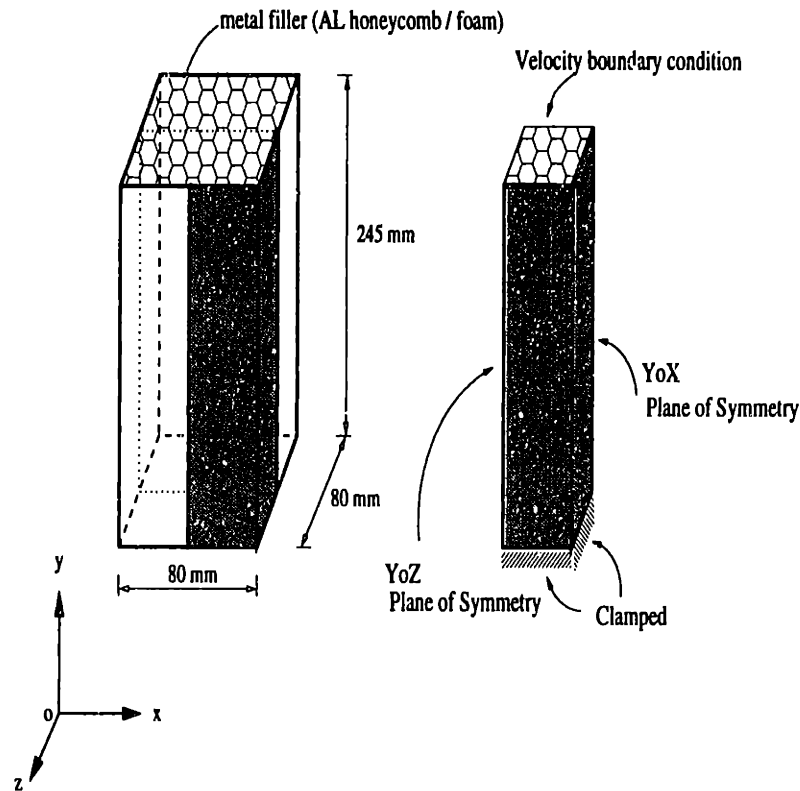


Figure 4.1: Square box column with honeycomb filler

model represented by a quarter box column was used to analyze this problem. A fine mesh with 10 elements in 60 rows was chosen to model each side of the column wall. Finite element model for a quarter box column was then comprised of 1200 shell elements.

A coarser mesh was chosen to model the filler. This mesh selection is due to the fact that computational time for 8-node continuum solid element is very high. In this numerical analysis, the mesh size for solid element was 5 by 5 elements in 30 rows. Finite element model for metal filler was then represented by 750 solid elements.

4.2 Geometric boundary conditions

Geometric boundary conditions for finite element analysis involved nodal displacement constraints applied on four different sections. As shown in Figure 4.1, clamped boundary conditions were applied at the bottom of the column (111111), while the top section of the column was only allowed to move in the axial direction (101111). On the $Y\text{-}O\text{-}Z$ plane of symmetry, the displacement in the x direction, rotation in the y and z axis were fixed (100011), while on the $Y\text{-}O\text{-}X$ plane, the displacement in the z direction, rotation in the x and y axis were restrained (001110).

4.3 Contact interfaces

Modeling contact interface between column wall and metal filler is a key point in achieving proper lateral strengthening effect. Two types of contact interfaces were used for sliding condition, namely self impacting contact type 36 and segment to segment contact type 23. Tied contact type 2 with failure was incorporated to model the adhesive.

4.3.1 Sliding interfaces

Self impacting contact type 36 was applied on the box column when the folding has developed. Self contact interfaces require the definition of only one surfaces. In this case, portions of wall surface may contact each other at initially unknown locations. Segment to segment contact type 23 was applied to capture interaction between the column wall and metal filler. This type of contact allows two interfaces, i.e. *master* and *slave* surfaces, to slide with respect to each other, but as soon as the structural reactive forces pull the interfaces apart then the interfaces will loose contact. In this study, initial gap of 1.06

mm was introduced between the column wall and metal filler to avoid infinite contact force interaction at the initial numerical simulation. Considering the column wall thickness was 1.88 mm , the dimension of the filler was then $76 \times 76 \times 245\text{ mm}$.

Contact interface type 23 and 36 are based on the *penalty* formulation, where geometrical inter-penetration between contacting faces are penalized by counteracting forces that are in essence proportional to the penetration depth. Hence, defining a suitable penalty parameter value is needed. Other important parameters which also need to be considered are friction condition on the interface, contact search accelerator, thickness of master and slave segments. For this simulation, frictionless contact condition between metal filler and thin-walled column was considered.

Contact search frequency accelerator (NACC) represents the number of time steps between contact slave searches. Both NACC and contact thickness of master and slave segments are critical in determining the depth of penetration allowed during the deformation on the contact interaction. If the NACC and the contact thickness are set too large, the penetration between two segments will be too large so that the penalty parameter can not have enough force to spring back the penetrated interfaces to their compatible contact condition. The default value of NACC in PAM-CRASH is 20. It also automatically calculates the default value for the contact thickness as shadow distance of $0.25 \sqrt{A}$, where A is the segment surface area. Since the nature of the folding mechanism of the column is in the deep collapse, the NACC value equal to 1 is needed. With this choice, contact search and update are done in every time step calculation. Meanwhile, the default value of contact thickness is adequate to run this type of problem.

The default value for penalty parameter is 0.1. If the penalty parameter for a given structural problem is too small, the resulting contact force is not enough to bring back the contacting faces into its compatible condition. As a result, an overlapping (inter penetration) between two segments will be obtained. For particular problem considered in this study, the default value of penalty parameter works very well for interface with self contact type 36, but it doesn't work for segment to segment contact type 23.

There are several indicators to check whether the penalty parameter value is suitable for certain structural modeling problem. The incompatibility on the contacting surface are indicated by the following structural response :

- Contacting segment overlapping each other. This indicates that penalty parameter is too soft so that the resulting contact force can not spring back the slave segment to its compatible position with master segment. A higher penalty parameter is needed for this case. A penalty parameter value of 0.1 will give this type of incompatibility for running metal filling column.
- Local deformation on contacting segment fall apart excessively. This indicates that the value of penalty parameter is too high. A smaller penalty parameter is needed for this case. A penalty parameter greater than 5 will result in this type of incompatibility.
- Contact force fluctuates excessively on subsequent deformation process. Contact force response needs to be checked even though the previous two indicators show compatible result. Small variation of contact force is acceptable due to incompatibility of deformation pattern resulting from coarse meshing. But, if contact force jumps to unreasonable value, it indicates that contact interfaces are not compatible. A penalty parameter value of 2.0 still gives this type of incompatibility.

After several simulation and utilizing the three indicators above, a penalty parameter value of 1.50 was found as adequate to run the simulation of thin-walled column filled with metal filler.

4.3.2 Tied contact

The presence of adhesive for bonding between metal filler and the column was modeled with tied contact type 2. In contrast with the sliding interface, tied contact uses kinematic constraint condition. Gap between two segments is tolerated, but adequate contact thickness should be incorporated to have both interfaces bonded.

Tied contact type 2 can capture failure mechanism due to excessive tension and shearing force on the contacting surfaces. Once the tied contact has failed at particular segments or nodes, the contact cannot be re-established whenever they come into closure during subsequent deformation process. Since the box column will undergo deep collapse deformation, re-establishing contact for segments failed from tied contact type 2 with sliding interface type 23 is needed in the numerical simulation.

4.4 Time step and mass scaling

Time step size for the dynamic explicit time integration needs to be chosen such that the computational stability holds. The time step required for stability in PAM-CRASH, [22], for shell and solid element are computed as follows :

$$\Delta t_{shell} = k \text{ MIN} \left(\frac{L}{\sqrt{E/\rho}} \right) \quad (4.1)$$

$$\Delta t_{solid} = k \text{ MIN} \left(\frac{L}{v + \sqrt{\frac{\lambda + 2G}{\rho} + v^2}} \right) \quad (4.2)$$

where k is the scale factor for the time step, L is the characteristic length of element, v is bulk viscosity characteristic, λ is the Lamé coefficient, G is the shear modulus, and ρ is the mass density of material. The numerical simulation will choose the smallest value between Δt_{shell} and Δt_{solid} .

Considering the time step variables in equation (4.1)–(4.2), the size of time steps can be set depending upon the time step scale factor k and mass density ρ , provided that the mesh size is already fine enough. Since the element size for the thin-walled column was smaller than the element size for metal filler, the time step size for this analysis was then solely controlled by the time step of shell element. Mass density has to be scaled down to run numerical simulation on the axial crushing of thin walled-column. After several simulation, mass density of $\rho = 2.7 \times 10^{-9} \text{ kg/mm}^3$ and time step scale factor $k = 0.9$ appeared to be sufficient to have computational stability.

4.5 Velocity boundary condition

To obtain the force – displacement response on the axial crushing of filled box column, velocity boundary condition was applied on the top portion of the column. Velocity was ramped during the first 50 microseconds to reach constant velocity of 2 m/s. The column was then compressed 75% to reach its effective crush length.

4.6 Material Properties

4.6.1 Aluminum extrusion properties

The box column was made from aluminum extrusion *AA 6063 T7*, which is commonly used for automotive structure. Mechanical properties for this type of material was obtained from [23] with Young's modulus $E = 6.9 \times 10^4 \text{ N/mm}^2$, initial yield stress $\sigma_y = 86.94 \text{ N/mm}^2$, and mass density $\rho = 2.7 \times 10^{-6} \text{ kg/mm}^3$. The strain hardening data are given in Table 4.1.

Table 4.1: Strain hardening data for AA 6063 T7

Plastic Strain	Plastic Stress [Mpa]	Plastic Modulus [Mpa]
0.0000E+00	0.8694E+02	0.3339E+05
0.2696E-03	0.9594E+02	0.2913E+04
0.2110E-02	0.1013E+03	0.2200E+04
0.5746E-02	0.1093E+03	0.1959E+04
0.1493E-01	0.1273E+03	0.1460E+04
0.2630E-01	0.1493E+03	0.5941E+03
0.6939E-01	0.1695E+03	0.1800E+02
0.1527E+00	0.1710E+03	0.0000E+00

4.6.2 Aluminum honeycomb properties

Aluminum honeycomb was used as one alternative of metal filler. Solid material type 41 (solid for improved side impact barriers) of PAM-CRASH material library was used in the model. Following material type 41 formulation, mechanical properties for aluminum

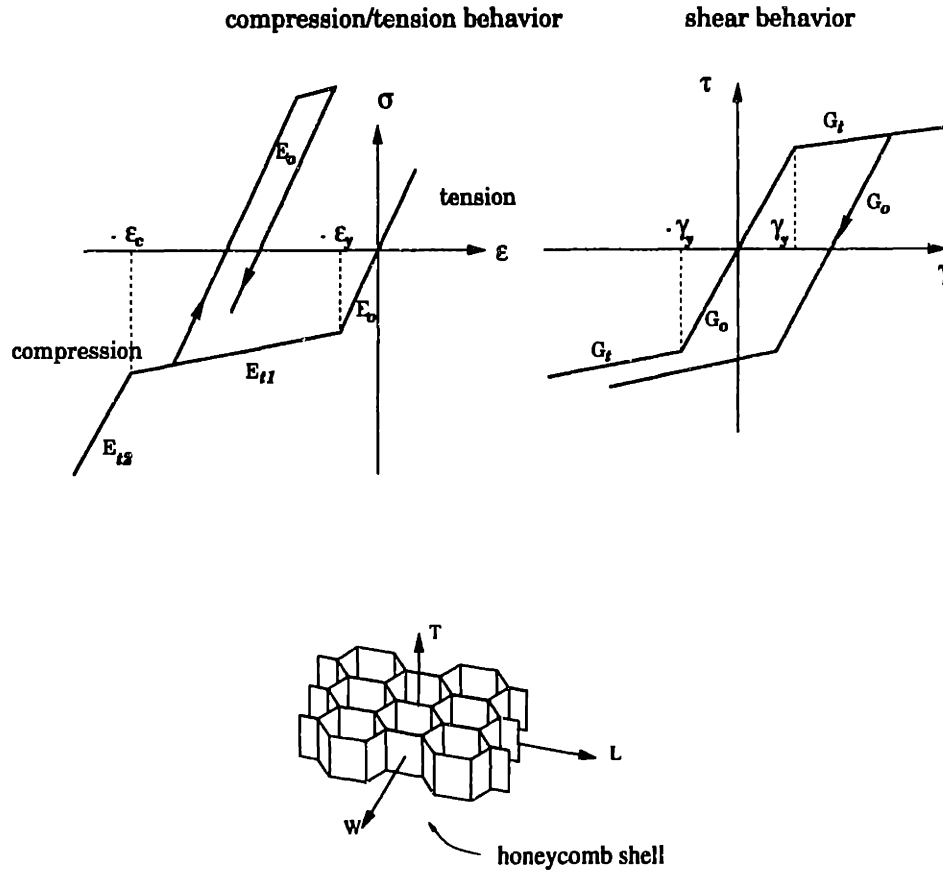


Figure 4.2: Constitutive modeling of material 41

honeycomb are smeared in T,L, and W direction. The direction T of the honeycomb is considered as the *strong axis*, while the direction L and W are considered as the *weak axis*. The definition of honeycomb axis and material 41 constitutive modeling are given in Figure 4.2.

Crash behavior studies with particular strengthening axis orientation were done on the aluminum honeycomb filling with the crushing strength of 0.345 MPa (50 psi). This low strength aluminum has a large size of honeycomb cells. Parameters of 3-D constitutive equations for this honeycomb were kindly provided by BMW R&D Center in Munich given in Table 4.2. The densification of aluminum honeycomb occurs at 80% crush distance.

Table 4.2: Mechanical properties of 0.345 MPa (50 psi) aluminum honeycomb

Properties	Normal T	Normal L	Normal W
E_o , Young modulus [Mpa]	17.6	1.75	1.0
ε_y , Compression yield strain	-0.02	-0.02	-0.02
E_{t1} , First tangent modulus [MPa]	0.15	0.001	0.001
E_{t2} , Second tangent modulus [Mpa]	10	10	10
G_o , Shear modulus [MPa]	22.41	0.5	16.0
γ_y , Shear yield strain	0.025	0.2	0.025
G_t , Shear tangent modulus [MPa]	0.01	0.1	0.5

4.6.3 Aluminum foam properties

In the case of aluminum foam with 50 psi crushing strength, all direction were assumed to have the same strong properties T. Thus, the existing material constitutive model of the honeycomb was used to described behavior of a foam under complex loading histories. The foam density of this particular crushing strength can be obtained by utilizing equation (3.27). In this equation, the theoretical prediction for aluminum foam crushing strength for HYDRO aluminum foam given in Table 4.3 will have a good correlation if the flow stress is taken to be $\sigma_o = 205MPa$.

Table 4.3: Mechanical properties of HYDRO aluminum foam

ρ_f [gr/cm ³]	0.16	0.26	0.31	0.40
σ_f [MPa]	2.1	5.9	7.1	10.9

4.6.4 Adhesive properties

The strength of adhesive is needed to specify failure criterion of bonding between metal filler and the column wall. Onset of failure is governed by the following failure criterion

$$\left[\frac{\sigma}{\sigma_{fail}} \right]^a + \left[\frac{\tau}{\tau_{fail}} \right]^b \leq 1 \quad (4.3)$$

where σ_{fail} and τ_{fail} are tensile and shear strength of the adhesive material, respectively. In the numerical simulation, the values for tensile and shear strength were taken to be $\sigma_{fail} = \tau_{fail} = 100 \text{ MPa}$, while the exponential constants were taken to be $a = b = 2$, as suggested by Seggewiss, [24].

Chapter 5

Simulation Results on the Crash Behavior of Filled-Box Columns

This chapter will first present the strengthening effect of strong mechanical properties orientation. Metal filler with crushing strength of 50 psi was used in this analysis. Numerical analysis will include two different studies in uni-directional and a hypothetical 2-D strengthening of aluminum honeycomb. The analysis will also study 3-D strengthening effect which can be obtained from aluminum foam filler. Four different numerical simulations were then performed on the axial crushing of filled box column. Crash behavior of filled box column for each strengthening orientation will be analyzed with regard to the crushing load, fold formation, energy absorption, and deformation pattern of the column wall. As a reference, crash behavior of filled box column will be compared with that of the empty box column.

This section will also present the crash behavior of filled box column with varying metal filler strength. Simple formulas for mean crushing load and specific energy absorption will be developed. Finally, numerical result will include the strengthening effect due to the bonding between metal filler and the column wall.

Total CPU time to run a complete crush analysis of an empty box column was approximately 5 hours in 175 Mhz *SGI O2* workstation. In the presence of metal filler, total CPU time increased to 10 hours. Moreover, total CPU time of 24 hours was needed to run the filled box column with adhesive.

5.1 Metal filler orientation

Four different type of simulations were run on the axial crushing of filled box column with different metal filler orientation :

- *Type 1* : Aluminum honeycomb filling with the strong axis aligned with the compression axis. In this case, the strong axis T was placed in the direction of y axis. The other weak axis L and W were then in the lateral direction of x and z axis.
- *Type 2* : Aluminum honeycomb filling with the strong axis placed perpendicular to the compression axis. In this case the strong axis T was in the lateral direction of z axis.
- *Type 3* : 2-D “hypothetical” aluminum honeycomb filling with strong axis placed in the lateral direction. In this case, one of the weak mechanical properties in L direction was replaced by the strong properties of T . The 2-D orthogonal strong axis of T were then aligned with the lateral direction of x and z axis, while the weak direction W was aligned in the compression axis y .
- *Type 4* : Aluminum foam filling with 3-D orthogonal strong mechanical properties. In this case, the weak properties in L and W were replaced by strong properties of T .

By strengthening the prismatic column in four different combinations, crash behavior of square box column with specific strengthening orientation can be studied further to obtain the optimum energy absorption.

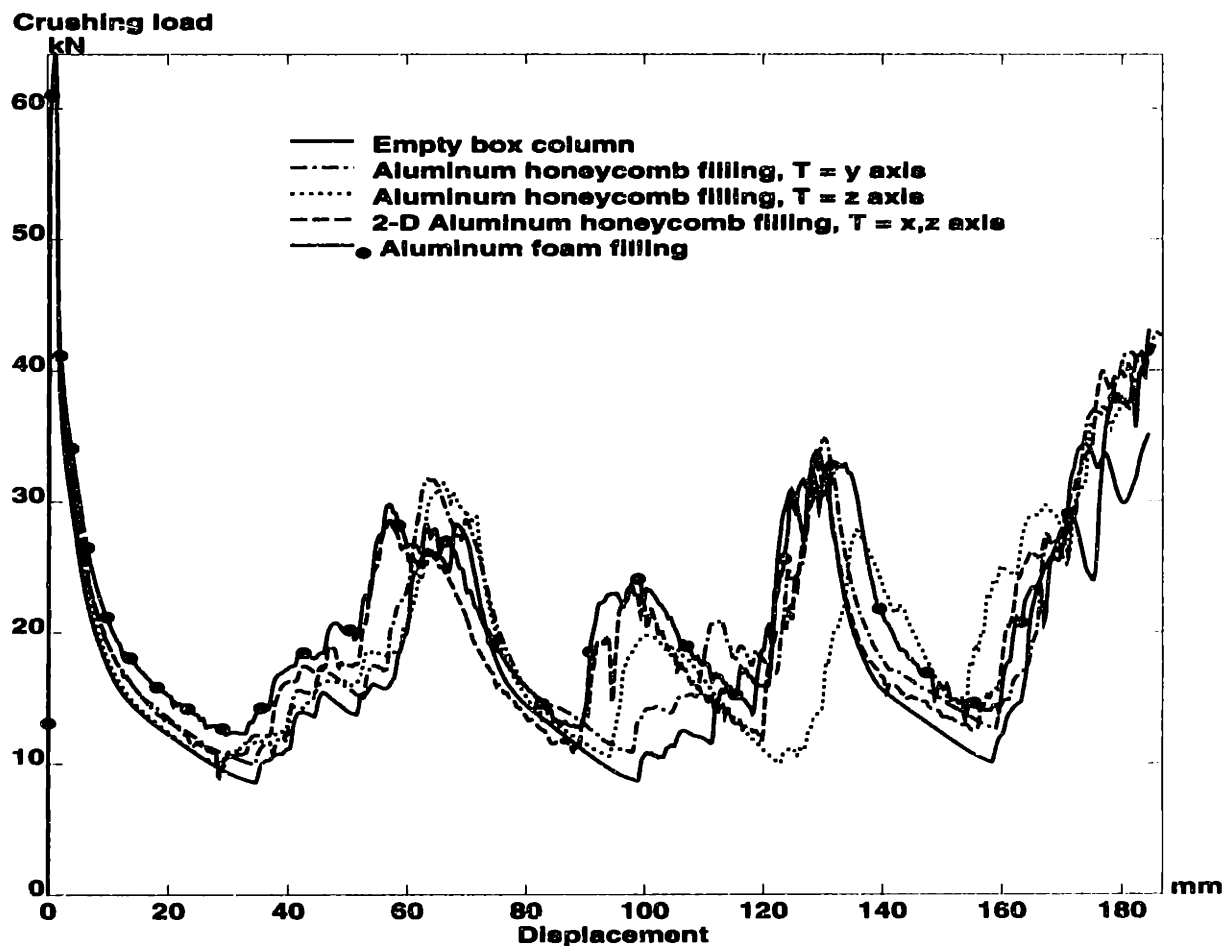


Figure 5.1: Crushing load characteristics for all types of filling (50 psi)

5.1.1 Crushing load and fold formation

Figure 5.1 presents crash response of aluminum honeycomb and aluminum foam filling. The strong axis of each metal filler has crushing strength of 50 psi. This is a relatively low strength reinforcement relative to the strength of an empty column. To obtain clear distinction on the crushing characteristics, all curves, except for empty box column, are filtered with *Sae1000 - 10*. Filtering subroutine is available in PAM-VIEWTM.

The distance between two peak loads correspond to the folding length. It can be seen that the folding length shifts to a shorter distance from empty box column to aluminum foam filling. The first peak load, which corresponds to the local buckling initiation, for all types of strong axis orientation needs almost the same value as the empty box column case at approximately 63 kN. This is due to the presence of the gap between the column wall and the filler. It appears that the first local plate buckling occurs before the strengthening of metal filler takes effect. By the time the column wall closes the gap, the load is already decreasing. The last peak on the load-displacement diagram corresponds to the formation of last fold and subsequently the densification of box column and metal filler. It is obvious from this figure that the aluminum foam filling gives the highest crushing load among the four different types of reinforcement. The effect of each strengthening orientation will be analyzed in greater detail.

Figure 5.2a shows axial strengthening of aluminum honeycomb filling in type 1 simulation. The plot of crushing load over the shortening in Type 1 simulation is quite similar with that of the empty box column. The crushing load characteristics show that a complete formation of one lobe for both Type 1 simulation and empty box column occur at approximately 60 mm. This finding can be explained by the fact that the honeycomb structure in this type of orientation ($T = y$ axis) only strengthen the axial compressive direction. The weak properties of aluminum honeycomb in L and W direction is so small that the lateral properties for empty and filled box column virtually remain the same. As a result, the formation of the folds will have the same characteristic of length for both cases. As the box buckle locally to form the subsequent folds, the filled column needs a higher crushing load due to the additional axial strengthening.

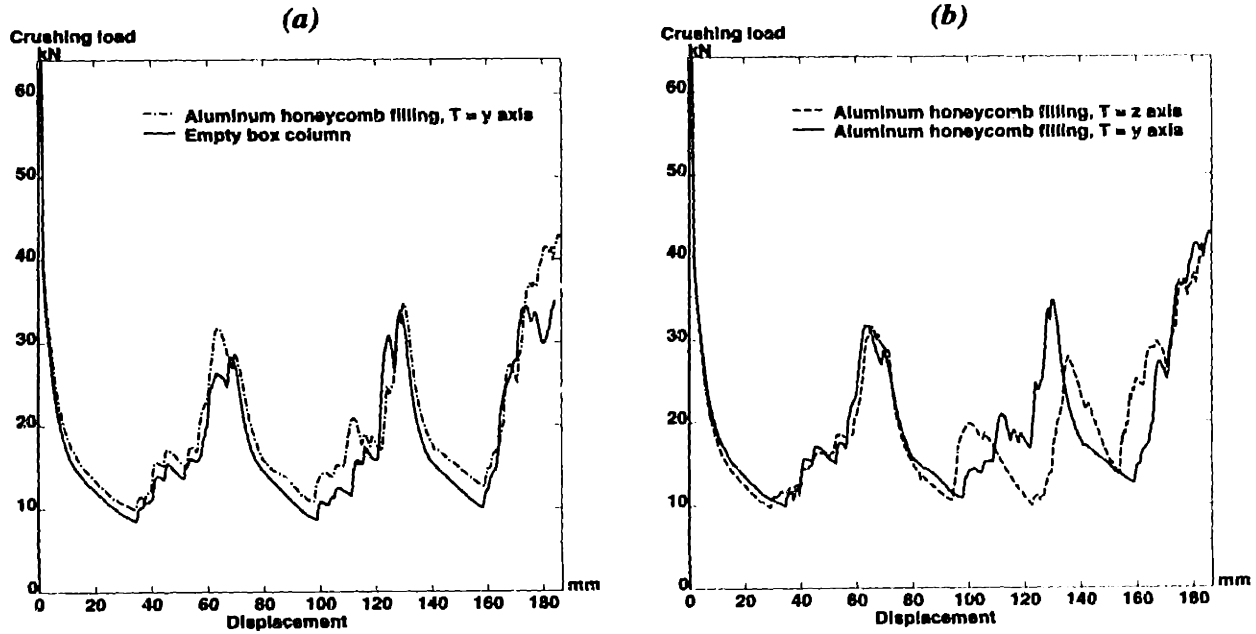


Figure 5.2: Unidirectional strengthening with aluminum honeycomb filling

Figure 5.2b depicts crushing load characteristics of filled box column for lateral strengthening in type 2 simulation. The crushing load is smaller than that of Type 1 simulation. Compared to empty box column, crushing load of Type 2 simulation is still higher even though the column does not get additional strength in the axial direction. The additional strength is caused by the change in the folding mechanism. The honeycomb filling increases the lateral strength of the column, which in turn restrains the formation of inward fold in the z axis. The lateral strengthening mechanism will lead to the formation of shorter folding length in the z direction, which is observed in decreasing the distance between two consecutive peak loads, and then resulting in higher crushing load.

Figure 5.3a shows the strengthening of square box column in 2-D lateral direction with a hypothetical strong 2-D honeycomb filling of type 3 simulation. Both lateral direction in x and z axis were strengthened, but the axial properties remained unchanged. The crushing

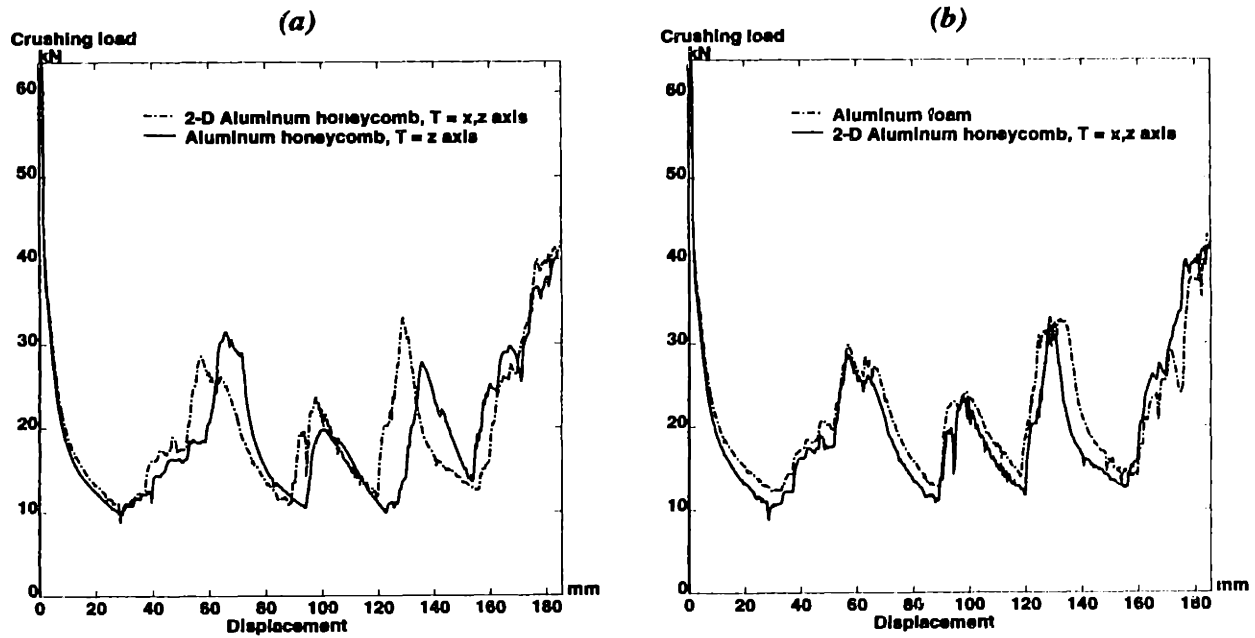


Figure 5.3: 2-D Lateral strengthening of box column

load curve for Type 3 is shifted from that of Type 2 simulation, leading to still shorter folding length and higher crushing load. The crushing load characteristics for Type 1 and Type 3 are almost the same. This characteristic will lead to a specific correlation between axial and lateral strengthening mechanism. More clear correlation will be observed in the analysis of energy absorption and mean crushing load on those types of simulation.

Type 4 simulation was run by giving additional axial strengthening to the case of Type 3 simulation. Thus, the box column was reinforced in all 3 orthogonal directions. For this purpose, aluminum foam can be considered as the filler. The crushing load characteristics for Type 4 and Type 3 simulation appear to have the same folding length as described in Figure 5.3b. This result reinforces the previous finding that the same lateral strength of the column will give the same folding characteristic. The additional strength is then obtained solely from the additional axial strengthening.

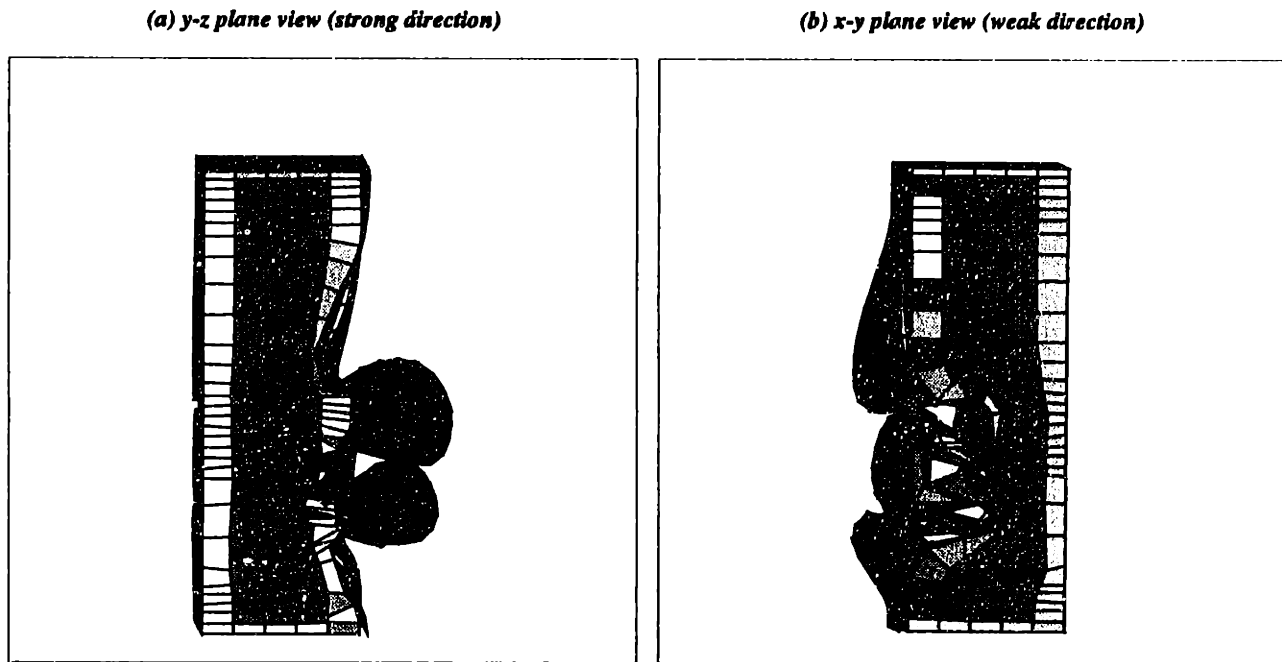


Figure 5.4: Deformation pattern of filled box column

5.1.2 Deformation pattern of filled-box column

The column deformation pattern of Type 1 simulation, which only strengthens the box column in axial direction, is similar to the deformation pattern of empty box column. The first inward fold is formed in the z axis direction for both cases, while the outward fold is formed in the x axis direction.

In contrast to the axial strengthening, the lateral strengthening changes the deformation pattern of the column wall significantly. Type 2 simulation represents uni-directional strengthening in z axis of the box column. Thus, the z direction can be referred as the *stronger axis*, and the x direction can be referred as the *weaker axis*. Placing the strong mechanical properties of metal filler in the weaker axis will prevent the formation of the inward fold in this direction. The numerical simulation confirms this folding behavior. The first inward fold is formed in the direction of x axis, while the first outward fold is formed in

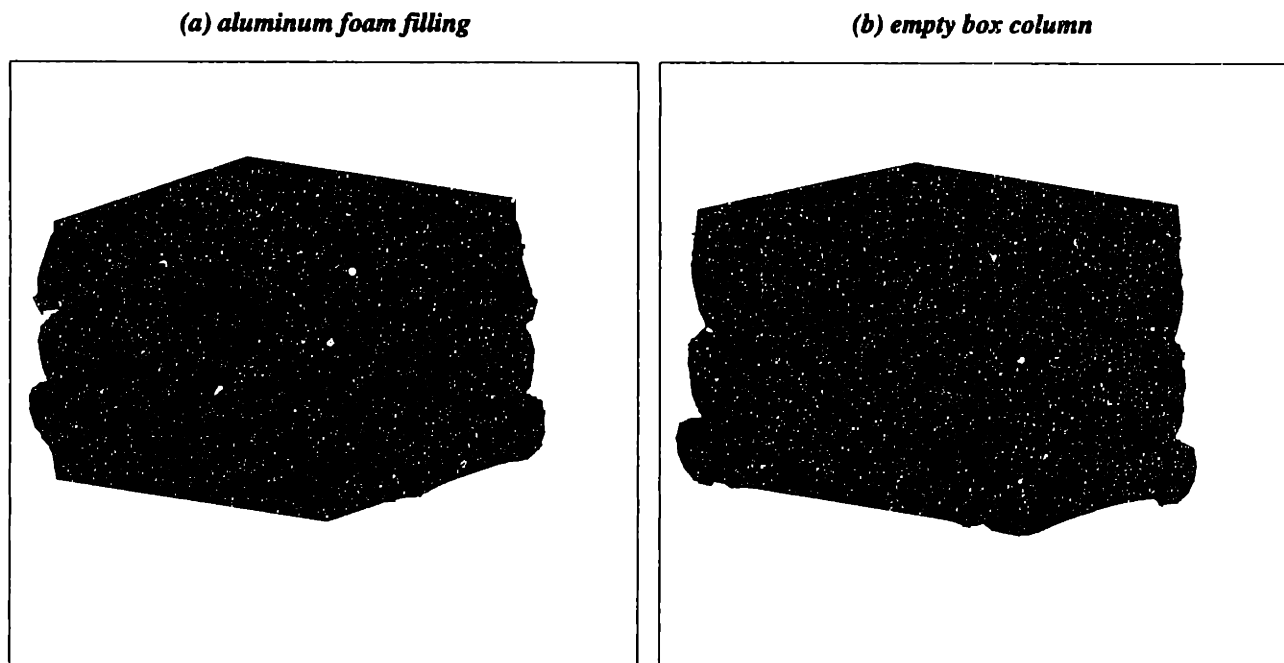


Figure 5.5: Deformation pattern of foam-filled and empty box column

the direction of z axis. In the subsequent deformation process, the inward fold formation in stronger axis is restrained by metal filler so that the depth of penetration of the column wall in this direction is less than that of in the weaker axis direction. This deformation pattern is shown in Figure 5.4. It shows that much deeper penetration of inward fold occurs in the weaker axis direction (Figure 5.4b) compare to the penetration in stronger axis direction (Figure 5.4a).

Lateral strengthening in two orthogonal direction will force the box column to have shorter folding length. As a result, more lobes are obtained when the lateral supports are applied to the column wall. As shown in Figure 5.5a, 3 lobes are formed in each side of the column wall. In empty box column, one side of the wall forms 2 lobes while the other side forms 3 lobes, as shown in Figure 5.5b. More lobes formation observed in foam-filled column is due to the shortening of the folding length. As a result, much higher crushing load is

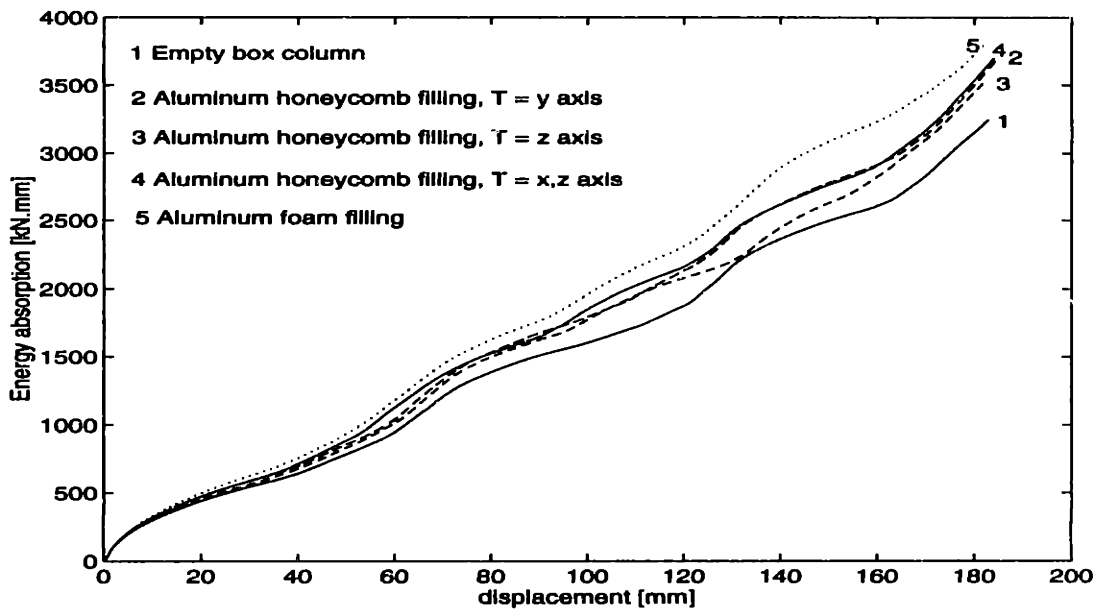


Figure 5.6: Energy absorption characteristics of filled-box column

needed to overcome more plastic folding in the column wall.

5.1.3 Energy absorption characteristics

Energy absorption of the box column takes place by extensive stretching and bending collapse of the column walls. By restraining the fold formation, which is followed by shortening the folding length, the column will absorb more energy. Figure 5.6 shows energy absorption characteristics for each type of simulation. The energy absorption plots are obtained by calculating the area under crushing load–displacement curve. As shown in that figure, the highest energy absorption is obtained by filling the box column with aluminum foam.

The energy absorption characteristics for aluminum honeycomb filling for $T = y$ axis is quite similar with $T = x, z$ axis. This finding will lead to the conclusion that the two

Table 5.1: Total energy absorption of filled-box column

Type of Column	Strong axis orientation	Energy absorbed E_b [kN.mm]	ΔE_b [kN.mm]	% Increase
Empty box column		3178.94		
Al honeycomb filling	$T = y$ axis	3532.66	353.72	11 %
	$T = z$ axis	3478.24	299.30	9 %
	$T = x, z$ axis	3566.89	387.95	12 %
Al foam filling	$T = x, y, z$ axis	3755.29	576.35	18 %

orthogonal lateral strengthening will increase the energy absorption by the same order as the axial strengthening of the box column.

The total energy absorbed by the filled-box columns undergo axial crushing load until reaching 75% crushing length are given in Table 5.1. From this table, an 18 % increase of energy absorption can be achieved through aluminum foam filling. On the other hand, aluminum honeycomb filling gives approximately 11 % increase of energy absorption which is achieved by strengthening the column in the axial direction.

5.1.4 Mean crushing load

Mean crushing load from the numerical analysis is defined by:

$$P_m = \frac{1}{\delta} \int_0^{\delta} P(\delta) d\delta \quad (5.1)$$

where $P(\delta)$ is the instantaneous crushing load corresponding to the instantaneous shortening δ . A plot of the mean crushing load over the shortening process for each type of simulation is given in Figure 5.7. It shows that after completing the first fold formation, the mean crushing

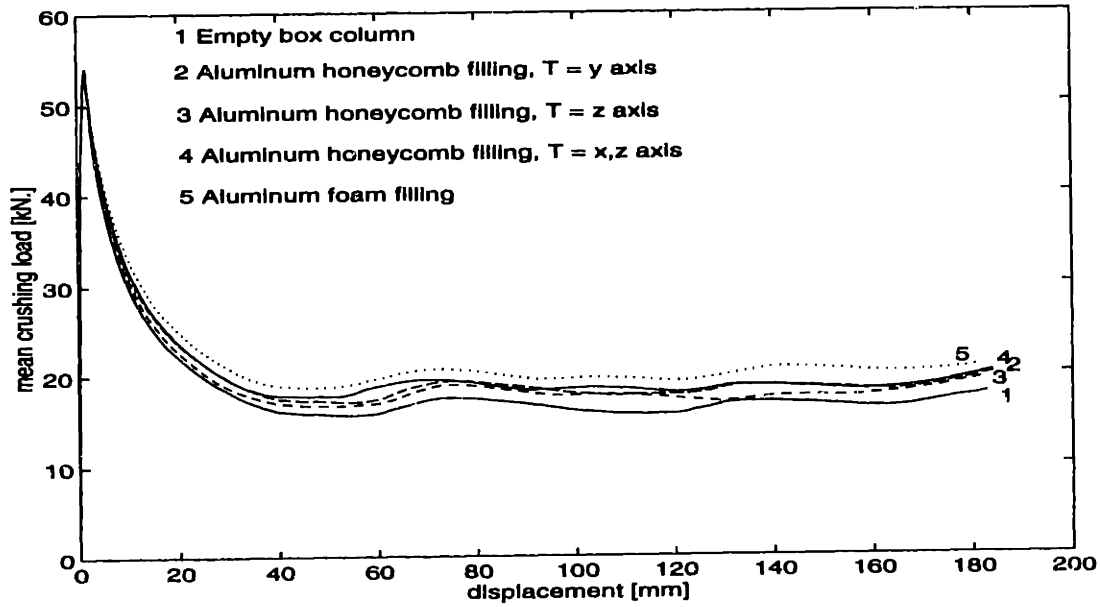


Figure 5.7: Mean crushing load of filled-box column

load oscillates around an asymptotic value with the decaying amplitude. The asymptotic numerical values for each type of simulation are given in Table 5.2.

From the asymptotic mean crushing load, it is seen that there is a clear similarity in strong axis orientation between uni-directional strengthening in y axis and two orthogonal strengthening in x and z axis. Both strengthening method gives the same mean crushing value of 18.6 kN. It is also obvious that in the uni-directional strengthening method, placing the strong axis in compressive direction is the best way to increase the mean crushing load. Mean crushing load of 16.9 kN for empty box column can also be obtained theoretically by using equation (3.5) if the flow stress is assumed to be $\sigma_o = 105.4$ MPa. Therefore, theoretical prediction in other problems involving the flow stress of the column will be based on this value.

Table 5.2: Asymptotic values of mean crushing load

Type of Column	Strong axis orientation	P_m [kN]	ΔP_m [kN]	% Increase
Empty box column		16.9		
Al honeycomb filling	$T = y$ axis	18.6	1.7	10 %
	$T = z$ axis	18.1	1.2	7 %
	$T = x, z$ axis	18.6	1.7	10 %
Al foam filling	$T = x, y, z$ axis	20.3	3.4	20 %
Theoretical prediction	empty box eqn.(3.5)	16.9		
	filled box eqn.(3.9)	18.8	1.9	11 %

Theoretically, the filled-box column increase its strength by 1.9 kN which compares favorably with numerically found value of 1.7 kN, which is obtained by axial strengthening of the column with honeycomb filling. By observing equation (3.9), the strength increase is obtained only by considering the additional compressive strength in the axial direction, while the strength in the lateral directions is ignored. An increase of 3.4 kN in the mean crushing load is obtained from the numerical analysis of aluminum foam filling. This value is twice compared to the increase of mean crushing force given by the axial strengthening of aluminum honeycomb filling. Scaling factor for these two different types of metal filler will be assessed further in the next section.

By considering the energy absorption characteristic and the increase of the mean crushing force, the optimum strengthening methods of the box column are obtained by using honeycomb filling with strong axis in the axial direction or aluminum foam filling. Even though the aluminum foam filling gives the best strengthening method, the aluminum hon-

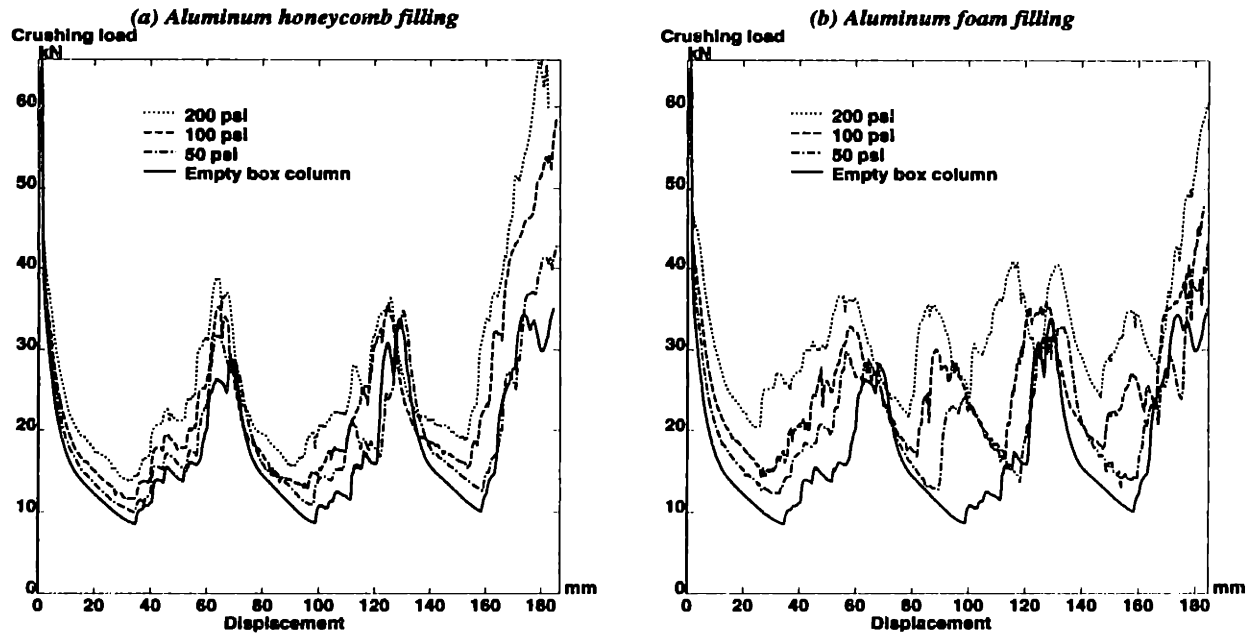


Figure 5.8: Crushing load characteristics for different strength of metal filler

eycomb filling method can not be ruled out. This is due to the fact that the additional weight for both methods has not yet been considered throughout the analysis.

5.2 Effect of crushing strength of metal filler

This section will present the crash behavior of filled box column with varying metal filler crushing strength. Numerical simulation were conducted on the filled box column with the optimum method of strengthening, i.e. aluminum honeycomb filling with strong axis in the axial direction and aluminum foam filling. Four different cases will be considered: empty box column and columns with 50 psi, 100 psi, and 200 psi filler. A simple theoretical prediction will be derived in the end of this section.

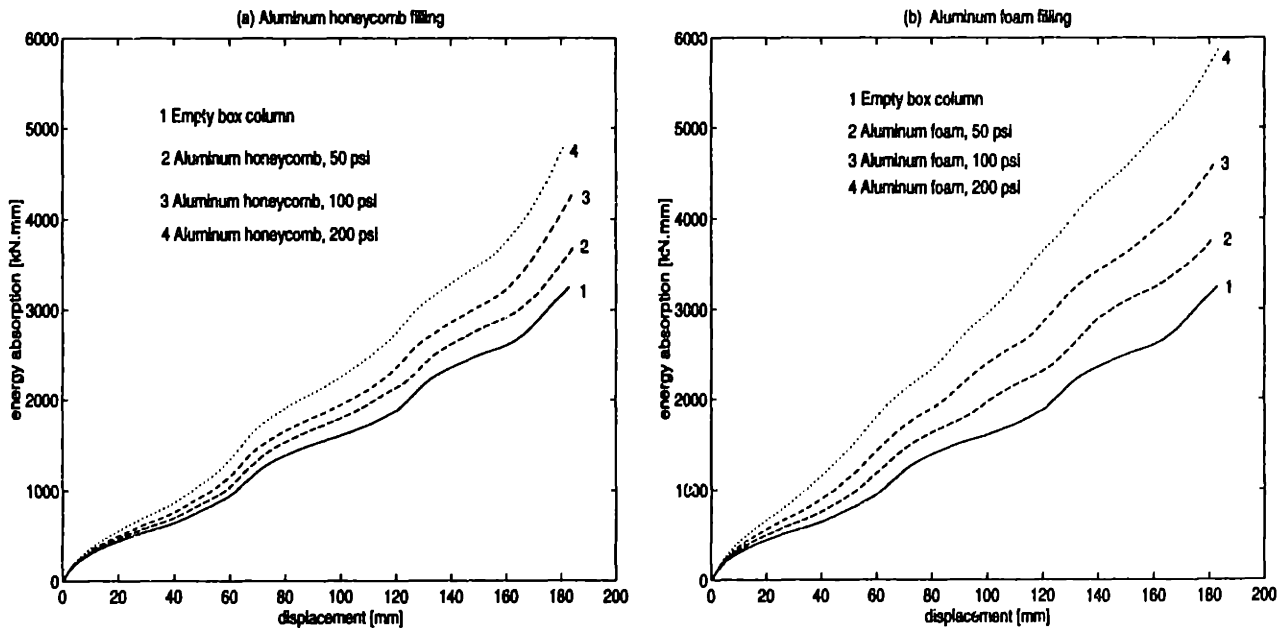


Figure 5.9: Energy absorption for different strength of metal filler

5.2.1 Crushing load characteristics

Figure 5.8a shows crushing load characteristics of aluminum honeycomb filling with different compressive strength. As observed in the preceding section, each crushing load curve is shifted vertically by a certain constant value. The distance between subsequent peaks is not affected by the honeycomb strength. This result confirms the previous analysis that, since the lateral properties unchanged, the fold formations for all three different compressive strength of aluminum honeycombs occur at the same crushing distance with the empty box column. The high peak load occurring at the end of crushing process is associated with the densification of the box column and aluminum honeycomb.

A different crushing load characteristics is obtained for aluminum foam filling with different compressive strength as shown in Figure 5.8b. The crushing load curves are shifted not only in the vertical direction, but also in the horizontal direction. The horizontal shift

corresponds to the shortening of the folding length with the increasing lateral strength of the column due to the aluminum foam filling.

Table 5.3: Total energy absorption for different strength of metal filler

Metal filler & strength [MPa] (psi)	Energy absorbed E_b [kN.mm]	ΔE_b [kN.mm]	% Increase
Empty box	3178.94		
Aluminum honeycomb			
0.345 (50)	3532.66	353.72	11 %
0.69 (100)	4096.65	917.71	29 %
1.38 (200)	4790.45	1611.51	51 %
Aluminum foam			
0.345 (50)	3755.29	576.35	18 %
0.69 (100)	4560.91	1381.97	44 %
1.38 (200)	5728.84	2549.90	80 %

5.2.2 Energy absorption characteristics

Figures 5.9a and 5.9b present the energy absorption characteristics for different metal filling strength. As the compressive strength of the aluminum honeycomb increase, the trend of energy absorbed by the column appears to be linear. A similar trend of energy absorption is observed for aluminum foam filling as depicted in Figure 5.9b. The total energy absorbed by the column during the crushing process (75 % crush) is given in Table 5.3. It shows that a significant increase in energy absorption can be achieved by filling the box column with aluminum honeycomb or aluminum foam. Aluminum honeycomb and aluminum foam filling

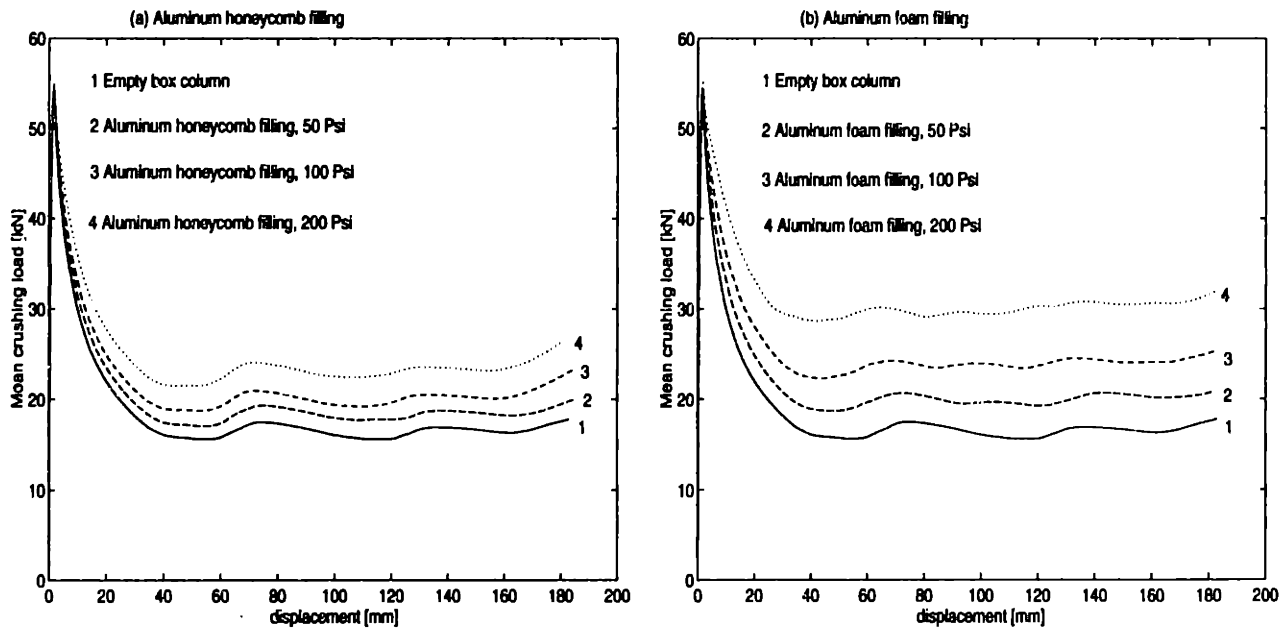


Figure 5.10: Mean crushing load versus crush distance for different strength of metal filler give an increase of energy absorption ranging from 11% – 51% and 18% – 80%, respectively. Considering the low weight of metal fillers, the increase of energy absorption in the box column is quite promising to be used as an alternative energy absorber.

5.2.3 Mean crushing load

Figure 5.10a and 5.10b show the mean crushing load of box column with different metal filler strength. From these figures, the asymptotic values of the mean crushing load show a linear dependence on the strength of metal filler. The asymptotic mean crushing loads are given in Table 5.4. This table shows that for a given metal filler strength, the additional mean crushing force ratio between aluminum foam filling and aluminum honeycomb filling is on the order of 2. This result confirms further that additional lateral support produces the strengthening effect in the same order as that of additional axial support of metal filler.

Table 5.4: Asymptotic values of Mean crushing load

Metal filler & strength [MPa] (psi)	P_m [kN]	ΔP_m [kN]	% Increase
Empty box	16.9		
Aluminum honeycomb			
0.345 (50)	18.6	1.7	10 %
0.69 (100)	20.3	3.4	20 %
1.38 (200)	23.7	6.8	40 %
Aluminum foam			
0.345 (50)	20.3	3.4	20 %
0.69 (100)	23.7	6.8	40 %
1.38 (200)	30.5	13.6	80 %

The scaling factor of 2 does not follow from the increase of energy absorption. The reason is explained below. In obtaining the energy absorption characteristic, one should integrate the crushing load–displacement curve. Since the number of peaks and troughs in aluminum foam filling curve is greater than that of in aluminum honeycomb filling, the area under the curve in each strengthening method of filling will then have non-linear relationship.

The mean crushing load values given in Table 5.4 also confirms the theoretical prediction for axial strengthening of the box column given in equation (3.9). In the case of structural foam, scaling factor of 2 is proposed in the theoretical prediction for calculating the mean crushing force. Thus, from this numerical result two formulas emerge for predicting the mean crushing force of filled box column, which are :

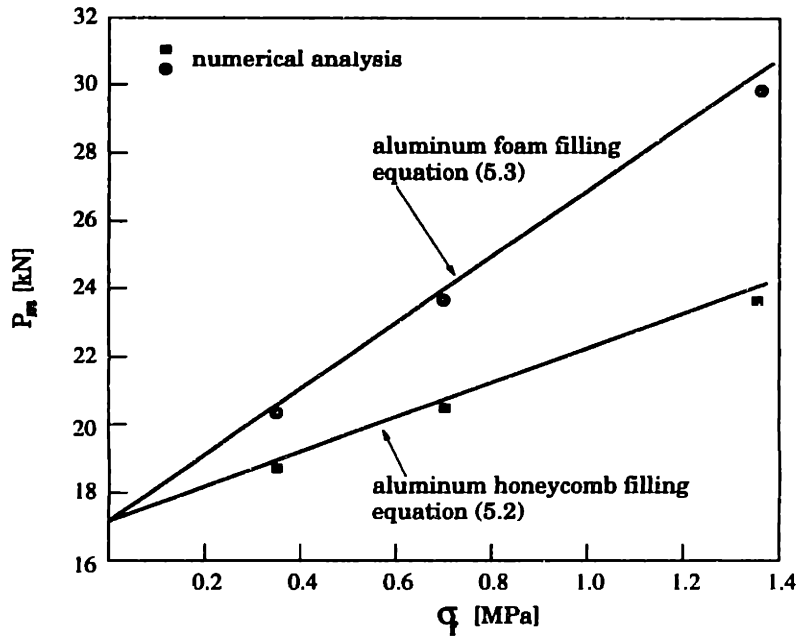


Figure 5.11: Mean crushing load for different strength of metal filler

for uni-axial strengthening using structural honeycomb filling :

$$P_{m,hcomb} = 13.05 \sigma_o t^{5/3} b^{1/3} + b^2 \sigma_f \quad (5.2)$$

for multi-axial strengthening using structural foam filling :

$$P_{m,foam} = 13.05 \sigma_o t^{5/3} b^{1/3} + 2b^2 \sigma_f \quad (5.3)$$

The numerical result and theoretical prediction given in equations (5.2) and (5.3) are plotted in Figure 5.11. Notice that theoretical predictions (solid lines) follow closely the numerical results.

5.3 Effect of adhesive

The presence of the adhesive for bonding between the foam and the column wall introduces considerable changes in the crash behavior of the system. First, the folding mechanism

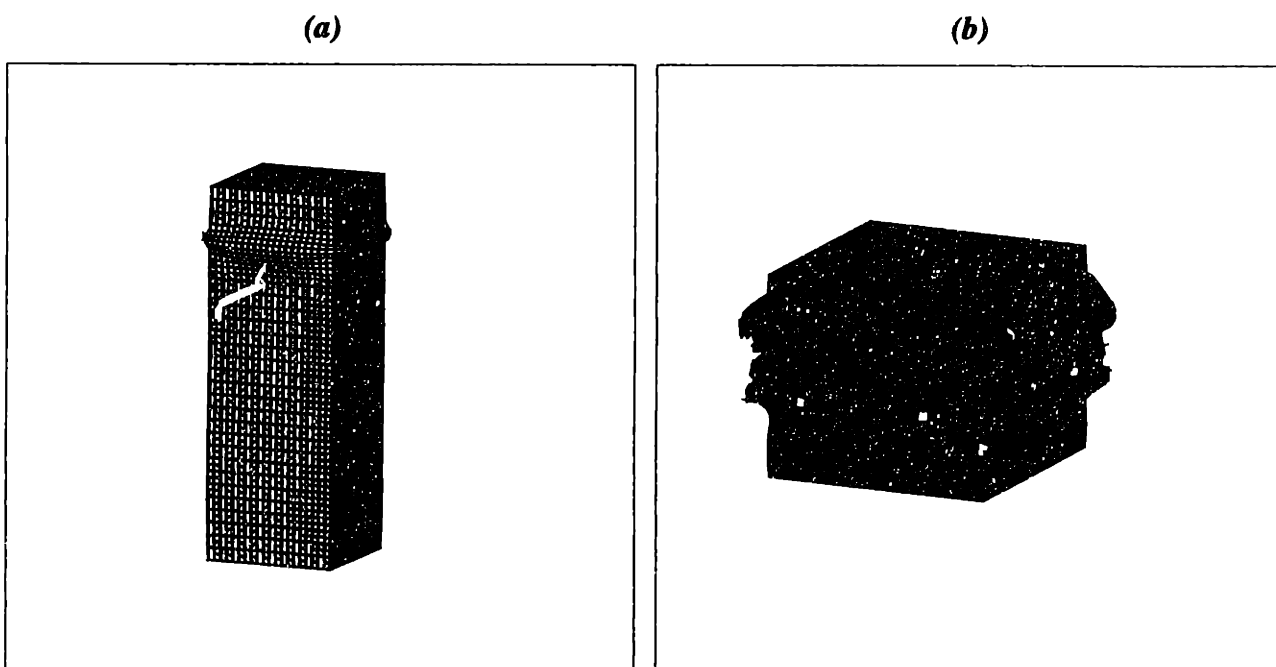


Figure 5.12: Symmetric (extensional) folding mode with adhesive without imperfections

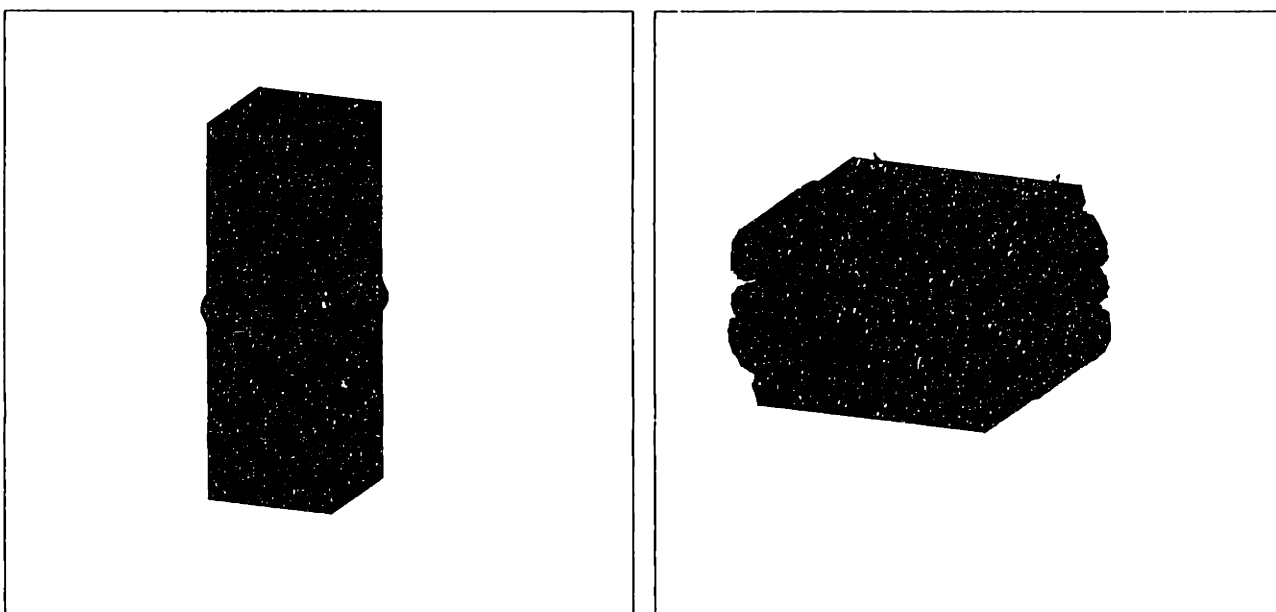


Figure 5.13: Asymmetric (quasi-extensional) folding mode with adhesive induced by triggering imperfection

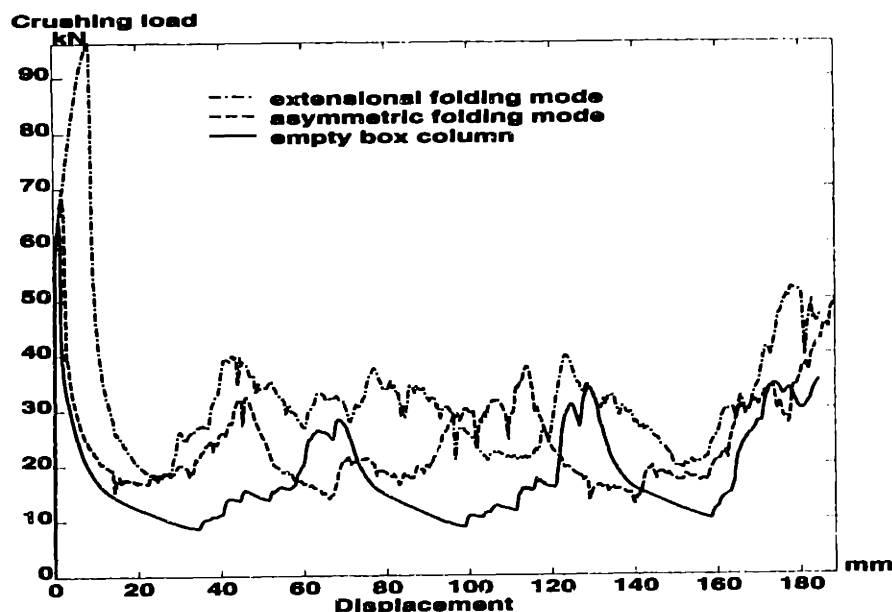


Figure 5.14: Crushing load characteristics for filled box column with adhesive

changes from the asymmetric (quasi-extensional) to the symmetric (extensional) mode (Figure 5.12). Secondly, the folding wavelength becomes much shorter. This is caused by additional restraining force on the formation of outward fold and also shear resistance produced by the adhesive material. The presence of adhesive material restrains not only the formation of outward fold, but also sliding between the column wall and metal filler. Smaller lobes are obtained in the extensional folding mode. It is interesting to note that the asymmetric, quasi-extensional mode of deformation can still be enforced in the column with the adhesive by introducing a triggering mechanism. The first asymmetric fold formation at the trigger location is shown in Figure 5.13a. A completely crushed column in the asymmetric folding mode is shown in Figure 5.13b. Notice that the lobes curvature for asymmetric folding mode is larger than the lobes curvature for extensional folding mode.

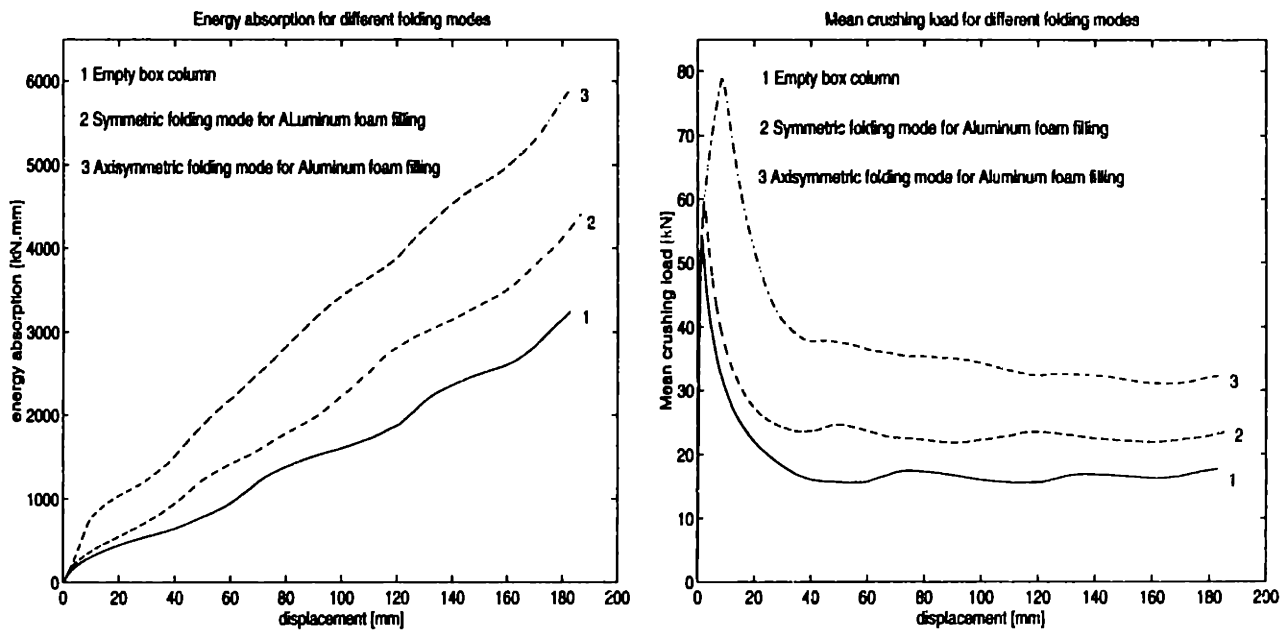


Figure 5.15: Energy absorption and mean crushing load with adhesive

5.3.1 Crash behavior characteristics

The crushing load characteristic for two different folding modes described above are shown in Figure 5.14. At the initial fold formation, the extensional folding mode is associated with a very high crushing load of approximately 97 kN. Compared to empty box column and no adhesive filling cases, the initial peak load for symmetric (extensional) folding accounts for almost 50 % increase. This initial high peak load is caused by the additional shear and extension strength provided by the adhesive which result in much stiffer column. On the other hand, the initial peak load for the asymmetric folding mode is approximately 68 kN, which accounts for 8 % increase from empty box column.

Figure 5.14 also shows that the crushing load characteristic has a larger number of peaks. In the asymmetric folding mode, the crushing load characteristics shows clear distinction between the peaks and the troughs. This can be interpreted that the column absorb energy

by forming outward and inward folds as indicated by the peaks and troughs, respectively. On the contrary, there is no clear distinction between the peaks and troughs on the crushing load characteristics of extensional folding mode. In this folding mode, the crushing load level is high for the entire deformation process. This high crushing load corresponds to the extensional outward fold formation. It can be inferred that in the case of extensional folding mode, the outward fold formation mode dominates the energy absorption process.

A plot of the energy absorption and the mean crushing force as a function of the column shortening is shown in Figure 5.15. The asymmetric folding mode increases the energy absorption by 31 % compare to the empty box column. A much higher increase of the order of 83 % of energy absorption is obtained by the extensional folding mode. The corresponding increase in the mean crushing force is 40 % and 81 %.

5.4 Specific energy absorption

This section will present the specific energy absorption which is usually used as an indicator for weight efficiency of a given cross-section. The effect of column length cancels out as discussed below. The specific energy absorption (*S.E.A.*) is defined by :

$$S.E.A. = \frac{\text{Energy Absorbed}}{m_c + m_f} \quad (5.4)$$

where m_c and m_f are column and metal filler weight, respectively.

Specific energy absorption for different metal filler densities are given in Table 5.5. The densities of aluminum honeycomb for weight calculation in Table 5.5 are taken from 5056 Hexagonal type produced by Hexcel Co., [19]. To obtain high specific energy absorption, aluminum foam with high strength to weight ratio must be used. For this purpose, the

density of HYDRO foam is used for weight calculation of aluminum foam filling. In the bonding problem, as suggested by [5], the weight of the adhesive amounts to 10 % of the total column weight.

Table 5.5: Specific energy absorption for filled box column ($b=80 \text{ mm}$, $t=1.88 \text{ mm}$)

Metal filler & strength [MPa] (psi)	ρ [kg/mm^3]	P_m [kN]	E_b [kN.mm]	$m_c + m_f$ [kg]	S.E.A. [$\frac{kJ}{kg}$]
Aluminum honeycomb	5056 alloy				
0.345 (50)	2.38×10^{-8}	18.6	3532.66	0.435	8.11
0.69 (100)	3.61×10^{-8}	20.3	4096.45	0.455	9.01
1.38 (200)	5.45×10^{-8}	23.7	4790.45	0.484	9.90
Aluminum foam	HYDRO foam				
0.345 (50)	4.09×10^{-8}	20.3	3755.29	0.456	8.23
0.345 (50)	adhesive-asym	23.7	4151.16	0.502	8.27
0.345 (50)	adhesive-exten	30.6	5805.36	0.502	11.56
0.69 (100)	6.49×10^{-8}	23.7	4560.91	0.490	9.31
1.38 (200)	1.03×10^{-7}	30.5	5728.84	0.544	10.54

Theoretical prediction for *S.E.A.* can also be made by using expression for the mean crushing force given by equations (5.2) and (5.3). The energy absorbed by the column can be obtained by multiplying the mean crushing force with the effective crush distance which is considered as 75% of the column height.

Consider the folding over one wave-length $2H$. The total weight of the column is $(\rho_c A_c + \rho_f A_f)2H$, and the effective crushing distance is approximately $\frac{3}{4}(2H)$ (see Chapter 2), where

A is the cross sectional area, and subscript c and f refer respectively to the column and metal filler. Combining equation (5.4) with equation (5.2) and (5.3), yields

$$S.E.A_{hcomb} = \frac{39.15\sigma_o(t/b)^{5/3} + 3\sigma_f}{16\rho_c(t/b) + 4\rho_f} \quad (5.5)$$

$$S.E.A_{foam} = \frac{39.15\sigma_o(t/b)^{5/3} + 6\sigma_f}{16\rho_c(t/b) + 4\rho_f} \quad (5.6)$$

In the limiting case where σ_f and ρ_f are zero, the expression given in equation (5.5) and (5.6) become the specific energy absorption for empty box column with varying thickness in the form :

$$S.E.A_{box} = 2.45 \frac{\sigma_o}{\rho_c} \left(\frac{t}{b} \right)^{2/3} \quad (5.7)$$

In terms of the total column weight m_t , the $S.E.A$ formulation for a given geometrical model (cross-section: 80 x 80 mm and thickness: 1.88 mm) can be obtained by substituting the crushing strength of metal filler for aluminum honeycomb and aluminum foam into the above formulation. Substituting equations (3.14) and (3.27) for the crushing strength of 5056 Hexcel honeycomb and HYDRO foam, respectively, into equations (5.5) and (5.6), one gets :

$$S.E.A_{hcomb} = \frac{3.1 + 97.4(m_t - 0.4)^{5/3}}{m_t} \quad [kJ/kg] \quad (5.8)$$

$$S.E.A_{foam} = \frac{3.1 + 49.9(m_t - 0.4)^{3/2}}{m_t} \quad [kJ/kg] \quad (5.9)$$

Similarly, the expression of S.E.A. for empty box column for a given geometrical model can be written as

$$S.E.A_{box} = 14.4 m_t^{2/3} \quad [kJ/kg] \quad (5.10)$$

The specific energy absorption does not have a unique value for each type of strengthening method. It depends on the density of filling material. The predicted values and numerical

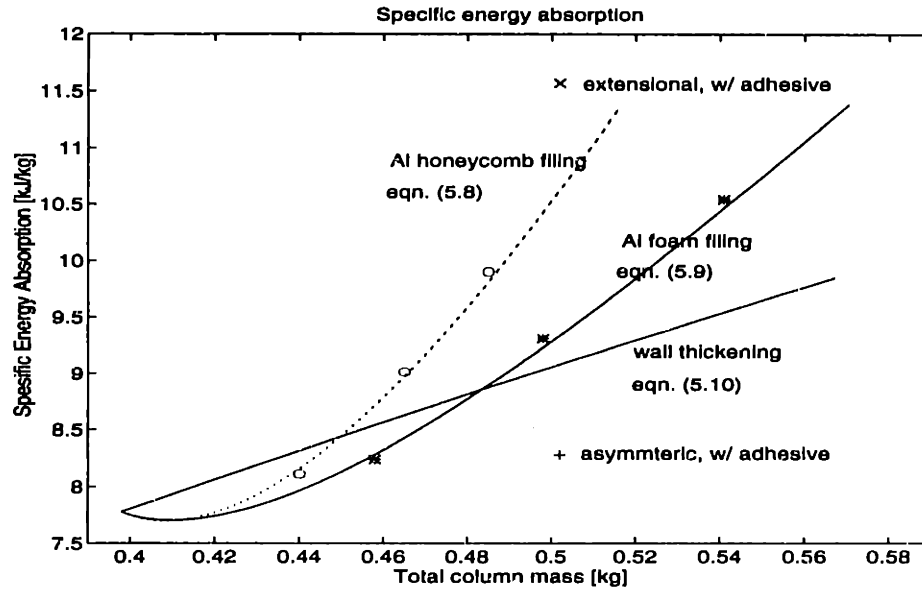


Figure 5.16: Specific energy absorption for different strengthening methods

results of specific energy absorption are plotted in Figure 5.16. Note that a starting point of all curves is the empty column with cross-sectional dimension of $80 \times 80 \text{ mm}$, 1.88 mm thickness, and 245 mm length. The theoretical prediction for specific energy absorption of each strengthening method is shown as smooth line, while the corresponding numerical results are shown as data points. The predicted values compare very well with the numerical results.

It can be seen that the *S.E.A.* can be divided into three different regions for the design consideration. The first region is the design for column with total weight less than 0.45 kg . In this region, thickening the column wall gives the best specific energy absorption. If the total column weight is in the range of greater than 0.45 kg , the aluminum honeycomb filling offers the highest specific energy absorption. This can be achieved by using aluminum honeycomb with the density greater than $3.2 \times 10^{-8} \text{ kg/mm}^3$. Thus, aluminum honeycomb

which has solidity ratio greater than 1.2 % gives the highest specific energy absorption.

The aluminum foam filling is superior to thickening of the column wall when the total column weight is greater than 0.485 *kg*. This strengthening method can be obtained when the aluminum foam density used in this design is greater than $6.15 \times 10^{-8} \text{ kg/mm}^3$. With this density, aluminum foam has the solidity ratio of 2.3 %. Note that by using adhesive for bonding, the folding mode changes and the foam can give as good energy absorption as the honeycomb does (see an isolated point corresponding to extensional folding mode with adhesive).

Chapter 6

Discussion and Conclusion

An efficient numerical procedure was developed to study the crash behavior of square box columns filled with aluminum honeycomb or foam. Interesting crash behavior are obtained from the numerical analysis. Some attractive results are the following:

1. Aluminum honeycomb filling with the solidity ratio greater than 1.2 % gives the highest strength to weight ratio.
2. Aluminum foam filling with the solidity ratio greater than 2.3 % gives higher strength to weight ratio compared to increasing the wall thickness of a box column. .
3. Aluminum honeycomb filling is more weight efficient than aluminum foam filling. A careful interpretation needs to be given to this finding which could only work for uni-directional loading. In a combination of compressive and bending problem, aluminum foam filling could give better crash behavior than aluminum honeycomb filling.
4. The additional lateral support produces a strengthening effect in the same order as that of the additional axial support in the filled box column.

Some conclusion regarding foam filling should be considered tentative until more rigorous constitutive modeling is developed for foam material. In the present paper, the foam was described by material 41 which has been developed for honeycomb. This material is based on fully uncouple behavior on the six components of stress and strain. Furthermore, honeycomb material adapted for foam carries an assumption that the ratio between compressive and shear strength of honeycomb is the same as that for foam. Additional test and/or theoretical development is necessary to confirm this hypothesis.

6.1 Selection of metal filler

The result outlined in the preceding section gives more information on how to design filled box column to obtain higher energy absorption. Metal filler with stiffer lateral direction will prevent inward fold formation. The lateral compressive strength will force the column wall to form shorter folding waves. At the extreme case when the lateral mechanical properties are very stiff, the column wall will form an extensional folding mode. Shorter folding length and extensional fold formation will lead to a higher crushing strength of the box column. This strengthening mechanism can be obtained from aluminum foam. The column material should have sufficient ductility to avoid premature fracture due to extensive tensile strains.

The strengthening to weight ratio superiority of aluminum honeycomb compare to aluminum foam is due to its lower density. For certain crushing strength, the density ratio between aluminum foam and honeycomb is on the order of greater than 3 (see equation (3.14) and (3.27)). In the same time, the ratio of strengthening effect on the column produced by aluminum foam and aluminum honeycomb filling is only on the order of 2. This density and strengthening scale factor leads to the superiority of aluminum honeycomb in

the specific energy absorption.

6.2 Effect of adhesive

The strengthening effect due to the bonding between the column wall and aluminum foam shows a significant increase in the energy absorption. But the total weight will increase significantly too. As reported in [5], the adhesive amounts to 5 – 16 % from the total weight of the filled column. The smaller the foam porosity, the less of the adhesive is needed for bonding between the column wall and the foam. Therefore, in the presence of adhesive, aluminum foam with smaller porosity will increase the specific energy absorption significantly. However, this result differs from that obtained in Ref. [5]. Two modeling simplifications on the foam material behavior and tied contact interface, which may lead to the different result, are given below.

Material type 41 used in PAM-CRASH numerical analysis captures plastic flow behavior in compression and shear mode (see Figure 4.2). It can only captures elastic behavior in the tension mode. On the other hand, the tension mode dominates the foam deformation in the presence of adhesive. Considering that the foam elastic limit is on the order of less than 2 % of the adhesive tensile strength, the foam must exhibit plastic deformation before the adhesive is failed. Moreover aluminum foam could crack and subsequently rupture at a low stress level before its tensile stress reaches the tensile strength of the adhesive, as shown by the study of Prakash *et.al.*, [25].

Bonding between the column wall and metal filer is easily simulated by using tied contact type 2 with failure. But right after bonding failure occurs, contact type 2 can not capture sliding interface when the segments come into contact in subsequent collapse mode. If contact

type 2 is the only contact interface applied in the contacting segments, the column wall and the filler will exhibit inter-penetration right after contact type 2 failures. In this analysis, the inter-penetration after failure is prevented by applying contact type 2 and contact type 23 in the beginning of simulation. This procedure has disadvantage that the column will have spurious lateral strength resulting from penalty stiffness of contact type 23.

The above deficiencies on the modeling of material and contact condition may explain the difference between numerical analysis and experimental results. In the experiments conducted by Hanssen and Langseth, [5], only a small increase of crushing load was observed in the presence of adhesive, leading to insignificant increase of the specific energy absorption.

6.3 Future study

Development of new material constitutive modeling for foam material which can capture plastic collapse and rupture behavior is needed. Furthermore, a new tied contact type which can capture sliding contact after failure needs to be developed.

Further study on the effect of metal filler to investigate the crash behavior of filled box column will provide a broad view of its crash absorption characteristics. Additional research should be done on the following group of problems :

- Contact interface variation between metal filler and the box column. If no adhesive is applied between metal filler and the box column, various sliding with friction condition need to be studied. If adhesive is applied between metal filler and the box column, a new tied contact which can capture sliding after failure need to be studied. The former case will give additional information on strengthening characteristic of the box column by studying the influence of friction between two different surfaces. Furthermore, the

latter case will give more information on the influence of adhesive in giving more additional strength of a box column.

- Study on the bending resistance of filled columns. In pure bending load, most of the energy is transferred to the lateral deformation of the column. Using and extending present finding on the lateral strengthening effect of the box column, study on the bending resistance can be used to investigate further the crash behavior characteristics on the application of low density metal filler.
- Crash behavior study on multi-cell columns filled with low density material. Unlike in single cell column, the partition plates will force multi cell column to form multiple folding at the same time. Study on the filling effect will give much needed insight into the strengthening characteristic of multi cell column.

Bibliography

- [1] Thorton, P.M., Mahmood, H.F., and Magee, C.L. Energy absorption by structural collapse. In Jones, N. and Wierzbicki, T., editors, *Structural Crashworthiness*, pages 96–117. Butterworths, 1983.
- [2] Wierzbicki, T. Crushing analysis of metal honeycombs. *International Journal of Impact Engineering*, 1:pp. 157–174, 1983.
- [3] Wierzbicki, T., Alvarez, A.L., and Hoo Fatt, M.S. Impact energy absorption of sandwich plates with crushable core. *Impact, Waves and Fracture*, AMD(205):pp. 391–411, 1995.
- [4] Kunze, H.D., Baumeister, J., Banhart, J, and Weber, M. Powder metallurgy technology for the production of metal foams. *Powder Metallurgy International*, 25(4):pp. 182–185, 1993.
- [5] Hanssen, A.G. and Langseth, M. Development in aluminium based crash absorption components. The Norwegian University of Science and Technology, N-7034 Trondheim, Norway. *Presented to the Norwegian–French Industry Conference in Paris*, November 1996.
- [6] Alexander, J.M. An approximate analysis of the collapse of thin cylindrical shells under axial loading. *Q.J. Mech. Appl. Math.*, 13:pp. 10–15, 1960.

-
- [7] Wierzbicki, T. and Abramowicz, W. On the crushing mechanics of thin-walled structures. *J. Appl. Mech.*, 50:pp. 727–739, 1983.
- [8] Abramowicz, W. and Jones, N. Dynamics progressive buckling of circular and square tubes. *International Journal of Impact Engineering*, 4:pp. 243–269, 1986.
- [9] Langseth, M. and Hopperstad, O.S. Static and dynamic axial crushing of square thin-walled aluminium extrusions. *International Journal of Impact Engineering*, 18(7–8):pp. 949–968, 1996.
- [10] Reddy, T.Y. and Wall, R.J. Axial compression of foam-filled thin-walled circular tubes. *International Journal of Impact Engineering*, 7(2):pp. 151–166, 1988.
- [11] Abramowicz, W and Wierzbicki, T. Axial crushing of foam filled columns. *International Journal of Mech. Sci.*, 30(3–4):pp. 263–271, 1988.
- [12] Santosa, S.P. and Wierzbicki, T. Crash behavior of box column filled with aluminum honeycomb or foam. Submitted to *Computers & Structures*, April 1997.
- [13] Gibson, L.J. and Ashby, M.F. *Cellular Solids: Structure and Properties*. Pergamon Press, Oxford, 1988.
- [14] Simone, A.E. and Gibson, L.J. Mechanical behavior of foamed aluminum. Technical report, Department of Civil Engineering, Massachusetts Institute of Technology, Cambridge, Massachusetts-02139, November 1996.
- [15] Abramowicz, W and Wierzbicki, T. Axial crushing of multicorner sheet metal columns. *Journal of Applied Mechanics*, 56:pp. 113–120, 1989.
- [16] Abramowicz, W. The effective crushing distance in axially compressed thin-walled metal columns. *International Journal of Impact Engineering*, 1:pp. 309–317, 1989.

-
- [17] Wierzbicki, T. and Abramowicz, W. The mechanics of deep plastic collapse of thin-walled structures. In Jones, N. and Wierzbicki, T., editors, *Structural Failures*. John Wiley, 1989.
 - [18] Wierzbicki, T. Crash behavior of foam-filled sections : An overview. Technical report, Impact and Crashworthiness Laboratory MIT, Cambridge, MA-02139, USA, January 1997.
 - [19] Hexcel. Mechanical properties of hexcel honeycomb materials. Technical report, Hexcel Structural Division, Dublin, CA-94568, USA, 1992.
 - [20] Gredestedt, J. L. Influence of cell wall wiggles on stiffness of cellular solids. Technical report, Department of Aeronautics, Royal Institute of Technology, S-100 44 Stockholm, Sweden, December 1996.
 - [21] Abramowicz, W. Crush resistance of t, y, and x sections. Technical Report 24, Department of Ocean Engineering, MIT, Cambridge, MA-02139, USA, January 1994.
 - [22] ESI Group Software Product Co., Paris. *PAM-CRASH User Manual*, 1996.
 - [23] Schneider, S. Energy absorption of extruded aluminum profiles in bending (in German). Master's thesis, Institute of Aeronautics, Universitat Stuttgart, Germany, 1994.
 - [24] Seggewiss, P. Numerical study of aluminum honeycomb structures (in German). Master's thesis, Department of Aerospace Engineering, Bundeswehr University, Germany, 1996.
 - [25] Prakash, O., Sang, H., and Embury, J.D. Structure and properties of Al-SiC foam. *Materials Science and Engineering*, A(199):pp. 195–203, 1995.